


Novel Clove Essential Oil Nanoemulgel Tailored by Taguchi's Model and Scaffold-Based Nanofibers: Phytopharmaceuticals with Promising Potential as Cyclooxygenase-2 Inhibitors in External Inflammation

This article was published in the following Dove Press journal:
International Journal of Nanomedicine

Reham Mokhtar Aman
Irhan Ibrahim Abu Hashim
Mahasen Mohamed
Meshali 

Department of Pharmaceutics, Faculty of
Pharmacy, Mansoura University,
Mansoura 35516, Egypt

Purpose: Clove essential oil is a phytochemical possessing a vast array of biological activities. Nevertheless, fabricating nano topical delivery systems targeted to augment the anti-inflammatory activity of the oil has not been investigated so far. Accordingly, in this study, controlled release nanoparticulate systems, namely nanoemulgel and nanofibers (NFs), of the oil were developed to achieve such goal.

Methods: The nanoemulsion was incorporated in the hydrogel matrix of mixed biopolymers – chitosan, guar gum and gum acacia – to formulate nanoemulsion-based nanoemulgel. Taguchi's model was adopted to evaluate the effect of independently controlled parameters, namely, the concentration of chitosan (X_1), guar gum (X_2), and gum acacia (X_3) on different dependently measured parameters. Additionally, the nanoemulsion-based NFs were prepared by the electro-spinning technique using polyvinyl alcohol (PVA) polymer. Extensive in vitro, ex vivo and in vivo evaluations of the aforementioned formulae were conducted.

Results: Both Fourier transform-infrared spectroscopy (FT-IR) and differential scanning calorimetry (DSC) established the complete dispersion of the nanoemulsion in the polymeric matrices of the prepared nanoemulgel and NFs. The ex vivo skin permeation data of clove essential oil from the prepared formulations showed that NFs can sustain its penetration through the skin comparably with nanoemulgel. Topical treatment with NFs (once application) and nanoemulgel (twice application) evoked a marvelous in vivo anti-inflammatory activity against croton oil-induced mouse skin inflammation model when compared with pure clove essential oil along with relatively higher efficacy of medicated NFs than that of medicated nanoemulgel. Such prominent anti-inflammatory activity was affirmed by histopathological and immunohistochemical examinations.

Conclusion: These results indicated that nanoemulsion-based nanoemulgel and nanoemulsion-based NFs could be introduced to the phytomedicine field as promising topical delivery systems for effective treatment of inflammatory diseases instead of nonsteroidal anti-inflammatory drugs that possess adverse effects.

Keywords: clove essential oil, biopolymers, Taguchi's model, nanoemulgel, nanofibers, anti-inflammatory activity

Correspondence: Irhan Ibrahim Abu Hashim
Department of Pharmaceutics, Faculty of Pharmacy, Mansoura University, El-Gomhoria Street, Mansoura, Dakahlia 35516, Egypt
Tel +20 1093008481
Fax +20502247496
Email irhanabuhashim@hotmail.com

Introduction

Recently, nanomedicine can breakthrough therapeutic methods and enhance medical understanding in accordance with traditional medicine. It is the application of nanotechnology to the field of medicine by utilizing materials at the nanometer scale. The

most common application of nanomedicine involves employing nanoparticulate systems to enhance the action of drugs in the prevention and treatment of diseases.¹ Lately, there has been an increasing trend in the nanoemulgel (NEG) and nanofibers (NFs) preparations.

NEG is an amalgamated formulation of two different systems in which nanoemulsion (NE) containing drug is incorporated into a hydrogel matrix.² Hydrogels can be prepared from natural or synthetic polymers. Natural hydrogels, prepared from natural polymers such as collagen, gelatin, chitosan (CS), guar gum (GG), gum acacia (GA) and alginate, are more advantageous than synthetic ones due to their biocompatibility, biodegradability, eco-friendly nature, low-cost production, plentiful raw resources as well as their use to design controlled release drug delivery systems (DDSs).³

A plenty of advantages were reported for application of NEG enumerated as follows: 1) it has a good adhesion property and spreadability on the skin compared to other topical DDSs as well as superior delivery of lipophilic drugs; hence, it is considered as a potential and promising candidate for enhancing the topical delivery of lipophilic drugs with improved patient compliance; 2) it controls the release of drugs having shorter half-life; 3) it is non-toxic and non-irritant; and 4) stability of NE is enhanced as a result of oil droplets distribution in gel base.²

More recently, electrospun NFs have been evaluated for their ability to serve as novel controlled release systems in pharmaceutical industries, especially topical and transdermal ones. This might be attributed to the fact that NFs size, surface area and porosity can be accurately controlled by varying different parameters. Electrospinning is the simplest and most efficient fabrication methods employed to produce NFs using solutions of naturally occurring biopolymers or synthetic polymers. Polyvinyl alcohol (PVA) is a biocompatible and nontoxic synthetic polymer with great electrospinnability. It has been widely applied for NFs preparation, either alone or blended with natural polymer (such as CS), as topical and transdermal scaffolds.^{4,5}

Phytochemicals are naturally occurring compounds found in plants that have versatile pharmacological activities against a variety of diseases.⁶ Amongst natural phenolic compounds that need to be incorporated in promising delivery systems is clove essential oil (CEO). CEO is an essential oil extracted from flower buds of *Syzygium aromaticum* L. (Family: Myrtaceae), recommended in the treatment of various diseases. Versatile pharmacological bioactivities including analgesic, antibacterial, antifungal, anti-allergic, anti-inflammatory, anticarcinogenic and antimutagenic activities have been

documented for CEO. Several phytochemicals have been identified in CEO, with the phenolic primary constituent being eugenol (88.85%) which is mainly responsible for most of the aforementioned biological activities of CEO (Figure 1).⁷

In spite of having versatile pharmacological activities, little trials to formulate and evaluate CEO in different delivery systems were reported. Antibacterial effects of clove essential oil nanoemulsion (CEO-NE) formulations were evaluated in comparison with pure CEO.⁷⁻¹⁰ Moreover, CEO was incorporated into the polyvinylpyrrolidone (PVP)-NFs mats using electrospinning process with the assistance of cyclodextrins (CDs) to prepare a fast-dissolving drug delivery system. Then, antifungal activity against oral fungi and cytotoxicity were evaluated.¹¹ Another study was implemented to investigate the antibacterial activity of essential oils including CEO that were incorporated in sodium alginate/PVA NFs by electrospinning technique.¹² These previously prepared NE and PVP-NFs mats systems exhibited fast release behavior and just in vitro antibacterial and antifungal activities were assessed. Consequently, different controlled release DDSs are still required to be constructed and evaluated to exploit and potentiate the versatile CEO pharmacological activities. Although documented lines of substantiation supporting the beneficial anti-inflammatory activity of CEO, a thorough review of literature disclosed that fabricating nano topical delivery systems targeted to augment the anti-inflammatory activity of CEO has not been so far studied.

Hence, the aim of this work was to develop controlled release nanoparticulate systems of CEO for topical application with potentiated anti-inflammatory activity and enhanced stability through NEG and NFs. Firstly, clove essential oil nanoemulsion (CEO-NE) was prepared and characterized. Secondly,

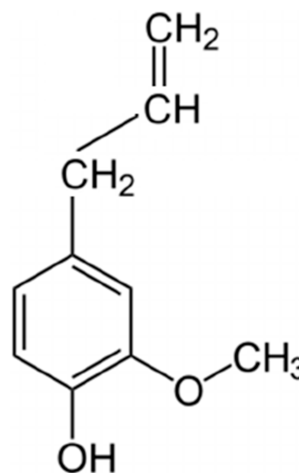


Figure 1 Chemical structure of eugenol.

blank hydrogel matrices of CS, GG and GA biopolymers were prepared and optimized by adopting Taguchi's model with three independently controlled parameters (ICPs) at three levels. Thereafter, both the optimized blank hydrogel and the CEO-NE formulae were selected for the preparation of CEO-NE-based NEG, which could be more suitable for better topical application. Thirdly, CEO-NE-based NFs mat was prepared by the electrospinning of CEO-NE and PVA. Ultimately, both NEG and NFs would be further characterized and extensively investigated.

Materials and Methods

Materials

CEO was obtained from Wako JAPAN, 036-03562, Lot KP J4110. Glycerol monoacetate (GMA) was acquired from Koch-Light Laboratories Ltd., Colnbrook Bucks, England. Polyoxyethylene (20) sorbitan monooleate (tween 80[®]) and croton oil were purchased from Sigma-Aldrich, Saint Louis, MO, USA while caprylocaproyl macrogol-8-glyceride (Labrasol) was obtained as a gift sample from Gattefossé, St Priest, France. PVA with a molecular weight (MW) of 146–186 kilodaltons (kDa) and a degree of hydrolysis of 98.0–98.8 mol % was purchased from Acros Organics, New Jersey, USA. Dimethyl sulfoxide (DMSO) with an MW of 78.129 g/mol was obtained from SDFCL, Mumbai-400030, India. GG was supplied by Premcem Gums Ltd., India while low MW CS (1526.454 g/mol) with a deacetylation degree of 90–95% was obtained from Oxford Chemical Co., Mumbai, India. Absolute ethyl alcohol, analytical grade of glacial acetic acid (99%), acetone, potassium phosphate monobasic (KH₂PO₄), disodium hydrogen phosphate (Na₂HPO₄), sodium chloride (NaCl) and GA were procured from El-Nasr Pharmaceutical Chemical Co., Cairo, Egypt. Primary anti-COX-2 (Polyclonal PA137504) was obtained from Thermo Fisher Scientific, Waltham, MA, USA while Universal kit [secondary antibody and 0.04% 3, 3'-diaminobenzidine tetrahydrochloride (DAB)] was procured from DAKO, Denmark.

Preparation of CEO-NE Formula

CEO-NE formula was prepared as previously reported with slight modification by using GMA instead of triacetin as an oil phase.⁷ It was obtained by mixing 1% w/w of CEO with GMA oil phase (8% w/w). The amount of surfactant (tween 80[®]): co-surfactant (Labrasol) mixture (S_{mix} (1:1)) (30% w/w) was added to CEO-GMA mixture

and finally water (61% w/w) was dropped to obtain an apparent and clear NE.

Characterization of CEO-NE Formula Physical Characterization

The prepared CEO-NE formula was subjected to thermodynamic stability studies; self-nanoemulsification efficiency tests; measurement of particle size, polydispersity index (PDI) and zeta potential (ZP) (using Malvern Zetasizer Nanoseries, Malvern Instruments Limited, UK); viscosity (η) measurement (using Cone and plate rotary viscometer, Haake Inc., Germany); drug content (%) as well as percentage transmittance (%T) estimation (using UV-VIS spectrophotometer, double beam, Labomed Inc., USA) and pH determination (using Calibrated potentiometer, Consort NV P-901 pH-meter, Belgium, Europe).

Fourier-Transform Infrared Spectroscopy (FT-IR)

The FT-IR spectra of pure CEO, CEO diluted in GMA (in a ratio of 1:8 as in the composition of CEO-NE), CEO-loaded NE, and its corresponding blank NE without drug were obtained using an FT-IR spectrophotometer (Madison Instruments, Middleton, Wisconsin, USA). The FT-IR analysis of pure NE components (namely; GMA, Labrasol and tween 80[®]) was also carried out using the same apparatus. The FT-IR spectra were recorded between 4000 and 400 cm⁻¹.

Transmission Electron Microscopy (TEM)

Transmission electron microscopy (TEM) was carried out using TEM (JEOL JEM-2100, JEOL Ltd, Tokyo, Japan). The CEO-NE formula was first diluted with deionized water, then dropped onto carbon-coated copper grid, and negatively stained with 2% phosphotungstic acid for 10 s. Whatman filter paper was used to draw-off the excess liquid and the prepared sample was blotted for dryness at room temperature. The sample was observed with TEM and the digital image was captured and analyzed using Digital Micrograph and Soft Imaging Viewer software.

Preparation, Characterization and Optimization of Blank Hydrogels Taguchi's Design of the Experiment

The design of experiment (DOE) using the Taguchi's model utilizes fractional factorial test design called orthogonal arrays (OA_S) that serve to reduce the number of experiments.⁸ The selection of a suitable orthogonal array (OA) hangs on the number of factors and their levels. For

instance, for three parameters at three levels, the conventional full factorial design would require 3^3 or 27 experiments. On the other hand, in the Taguchi L9 OA, the mandatory experiments are only 9 (F-1–F-9). Thus, the aforementioned performance improvement along with lower costs and time saving can be achieved following such design. Based on these outstanding merits, Taguchi L9 OA design (three factors with 3-level design) was applied in the current study for statistical optimization of blank hydrogel formulations and inspecting the effects of major factors on responses.

Effective Factors and Levels

Three ICPs, namely CS concentration (X_1), GG concentration (X_2) and GA concentration (X_3) were analyzed for their paramount influence on blank hydrogels characteristics (Table 1). The selection of these levels was based on initial trials and the optimization process was executed within such limits.

Selection of OA and Factor Assignments

In this research, L9 OA (three parameters, in three levels), where L and subscript 9 denote the Latin square and the number of the experimental runs, respectively, was used (Table 2). To observe the data reliably on experiment, pH and η at a shear rate (γ) of 192 s^{-1} (as dependently measured parameters (DMPs)), were repeated three times with the same conditions to attain the average. For statistical analysis of the results as well as conditions optimization, Minitab 18 Statistical Software[®] (Minitab Inc.) was used.

Signal-to-Noise Ratio ((S/N) Ratio)

With respect to the Taguchi's model, "signal (S)" and "noise (N)" for output attributes and the (S/N) ratio represents the desirable (S) value (arises from the ICPs) and the undesirable (N) value (originates from factors that cannot be controlled such as environmental factors). The (S), (N) and ((S/N) ratios) values are computed differently by the model into three different options: "larger is better",

Table 1 ICPs and Their Levels Used in L9 Taguchi OA Design

ICPs	Units	Levels		
		1	2	3
X_1 : Concentration of CS	% w/w	1	1.5	2
X_2 : Concentration of GG	% w/w	0.5	1	1.5
X_3 : Concentration of GA	% w/w	0	2	4

Abbreviations: CS, chitosan; GA, gum acacia; GG, guar gum; ICPs, independently controlled parameters; OA, orthogonal array.

Table 2 Formulations of Blank Hydrogels by L9 Taguchi OA Design

Formula No.	Formula Code (Levels)	Concentration (%w/w)		
		CS (X_1)	GG (X_2)	GA (X_3)
F-1	$C_1G_1A_1$	1	0.5	0
F-2	$C_1G_2A_2$	1	1	2
F-3	$C_1G_3A_3$	1	1.5	4
F-4	$C_2G_1A_2$	1.5	0.5	2
F-5	$C_2G_2A_3$	1.5	1	4
F-6	$C_2G_3A_1$	1.5	1.5	0
F-7	$C_3G_1A_3$	2	0.5	4
F-8	$C_3G_2A_1$	2	1	0
F-9	$C_3G_3A_2$	2	1.5	2

Abbreviations: CS, chitosan; GA, gum acacia; GG, guar gum; ICPs, independently controlled parameters; OA, orthogonal array.

"nominal is the-best", and "smaller is better", based on the category of the performance characteristics.^{8,13} The objective of this study was to prepare hydrogels with a suitable pH as well as acceptable η for topical application; hence, the quality characteristic goes for "larger is the better" for (S/N) ratio by the model.

After all of the (S/N) ratios have been computed for each run of an experiment, Taguchi recommends a graphical approach to analyze the data. In the graphical approach, the (S/N) ratios are plotted for each factor against each of its levels.

Statistical Analysis

Analysis of variance (ANOVA, general linear model) was implemented to analyze the paramount influence of each ICP on blank hydrogels characteristics (DMPs), namely pH and η at γ of 192 s^{-1} and to determine contribution (%) of each factor.

Preparation of Blank Hydrogels

Based on Taguchi L9 OA design, blank hydrogels were prepared by blending different concentrations of CS, GG and GA as summarized in Table 2. Briefly, CS was dispersed in 1% (w/w) aqueous acetic acid solution using overhead mechanical stirrer (T-line Laboratory Stirrer, Talboys Engineering, 230 V, 1250 rpm), at room temperature for 10 min to make up CS concentrations of 1, 1.5, and 2% w/w. Then, to maintain GG concentrations of 0.5, 1, and 1.5% w/w, it was sprinkled gently to the aqueous CS solutions while stirring for an additional 10 min. For hydrogels formulae containing GA, it was added gradually to attain its concentration at 2 and 4% w/w and stirring was continued

for 5 min (Table 1). Finally, the prepared hydrogels mixtures were magnetically stirred using magnetic stirrers (Thermolyne Corporation, Dubuque Iowa, USA) for 5 h at room temperature. The dispersions were sat aside overnight to form a gel.

Physicochemical Characterization of the Prepared Blank Hydrogels

Visual Examination

Blank hydrogels were inspected visually for their color, homogeneity (appearance and existence of any aggregates), grittiness (presence of grits or particles), and syneresis (phase separation).

pH Determination

The pH of various hydrogels formulae was measured using a calibrated potentiometer (Consort NV P-901 pH-meter, Belgium, Europe). The electrode was immersed into each freshly prepared formula 10 min prior to recording the reading at room temperature. Each measurement was performed in triplicate and presented as mean \pm standard deviation (SD).

Rheological Study

The rheological profile of the prepared blank hydrogels formulae was studied using a cone and plate rotary viscometer (Haake Inc., Germany). The η and the shear stress (τ) of the formulae were measured as a function of the applied γ . To enable the construction of η versus γ plots, experiments were conducted by changing γ between 192 and 384 s^{-1} through arbitrary varying the speed (n) between 32 and 64 rpm. The η , τ and γ are calculated according to the following Equations (1), (2) and (3):

$$\eta = \frac{G.S}{n} \quad (1)$$

$$\tau = A.S \quad (2)$$

$$\gamma = M.n \quad (3)$$

Where; η : Viscosity in millipascal.second mPa.s (mPa.s = 1 centipoise (cP)), G: Instrumental factor = 10^3 A/M (=14,200) (mPa.s/scale grad. min), S: Torque (scale grad.), n: Speed (rpm), τ : Shear stress in pascal (Pa), A: Shear stress factor (Pa/scale grad.), γ : Shear rate in reciprocal second (s^{-1}), and M: Shear rate factor (minute/second = min/s).

Formulations were carefully applied to the lower stationary plate of viscometer and the upper cone was adjusted.

Samples were then allowed to equilibrate for 5 min to attain the running ambient temperature before each measurement¹⁴ and to facilitate relaxation of internal stresses introduced during sample loading. Experiments were done in triplicate for each sample, and data were expressed as mean \pm SD.

Preparation and Characterization of CEO-NE-Based NEG

Incorporation of CEO-NE into the Optimized Blank Hydrogel to Prepare CEO-NE-Based NEG

Four and half milliliters of the prepared CEO-NE were diluted with water to a weight of 23.375 g NE.¹⁵ Glacial acetic acid (0.25 g) was added to the diluted NE to allow the subsequent dispersion of CS in the NEG. The components of the optimized F-9 hydrogel (CS 2%w/w, GG 1.5%w/w and GA 2%w/w) were then added to the diluted NE as previously described under preparation of blank hydrogels to finally prepare 25 g CEO-NE-based NEG.

Characterization of the Prepared CEO-NE-Based NEG

Visual Examination

The prepared CEO-NE-based NEG was checked for color, homogeneity, grittiness, and syneresis under normal daylight.

pH Determination

The pH of prepared CEO-NE-based NEG was measured using a calibrated potentiometer (Consort NV P-901 pH-meter, Belgium, Europe) as previously described for blank hydrogels.

Measurement of Viscosity

The CEO-NE-based NEG's η was measured using a cone and plate rotary viscometer (Haake Inc., Germany) at n of 32 rpm (γ of 192 s^{-1}) to determine the suitability of the prepared NEG for topical application.

Assay of Drug Content

A specific quantity (2 g) of the prepared CEO-NE-based NEG and its corresponding blank was weighed and dissolved in DMSO and 1% (v/v) aqueous acetic acid solution (10:90%) using an ultrasonic bath (Sonix USA, SS101H230) for 1 h. One milliliter absolute ethanol was added to each solution and the final volume was adjusted to 10 mL in a volumetric flask using the aforementioned solvent mixture. CEO content in each formula was estimated at 279 nm spectrophotometrically, using double beam UV-VIS spectrophotometer (Labomed Inc., USA),

against the corresponding blank solution. This test was performed in triplicate and drug content was calculated as mean \pm SD.

Fourier-Transform Infrared Spectroscopy (FT-IR)

Each polymer alone (namely: CS, GG and GA) and their physical mixture corresponding to the optimized blank hydrogel formula (F-9), as well as medicated NEG and its blank were subjected to FT-IR spectroscopy using FT-IR spectrophotometer (Madison Instruments, Middleton, Wisconsin, USA) in the range of 4000 to 400 cm^{-1} .

Differential Scanning Calorimetry (DSC)

Differential scanning calorimetric (DSC) thermograms of pure drug (CEO), CEO-NE and its blank, as well as medicated NEG and its blank were performed using a differential scanning calorimeter (DSC 6000, Perkin-Elmer, Waltham, MA, USA). Calibration was performed employing indium with a melting point of 156.6°C and purity of 99.99%. The samples were crimped in standard aluminum pans and heated over a temperature range of 35–350°C at a constant heating rate of 10°C/min under constant purging of dry nitrogen at 20 mL/min.

Preparation and Characterization of CEO-NE-Based NFs

Preparation of CEO-NE-Based NFs

Polymer (PVA)-CEO-NE Solution Preparation

PVA solution was prepared by dissolving PVA (10% w/w) in aqueous acetic acid (1% v/v) and heating at 80°C for 3 h to ensure complete dissolution of the polymer. After cooling to room temperature, the polymer solution was blended with CEO-NE at a ratio of (3:1 w/w) to keep PVA concentration constant at 7.5% w/w.⁴ The obtained mixture was magnetically stirred using a magnetic stirrer (Thermolyne Corporation, Dubuque Iowa, USA) for 2 h to ensure a homogeneous distribution and then the dispersion was immediately electrospun to prepare CEO-NE-based NFs.

Electrospinning Apparatus

An electrospinning setup described previously was used to electrospin the obtained dispersion.⁴ The electrospinning setup consisted of a syringe pump that could be adjusted to control the solution flow rates (0.1–60 mL/h), a grounded collector plate covered with aluminum foil and a high voltage power supply (0.5–30 kV, 0–50 μA current). An electrospinning apparatus (MECC CO., Ltd., JAPAN) was used in all experiments. The prepared dispersion of PVA: CEO-NE was

loaded into a 5-mL glass syringe with a blunt-end tip (stainless steel, 27 G) and the flow rate was 1.2 mL/h. The flow rate was determined empirically to obtain stable electrospinnable jets. The distance between the capillary tip and the grounded metal collector was 10 cm and a voltage of 20 kV was applied. These conditions were kept constant throughout all experiments. CEO-NE-based NFs were kept at -18°C for overnight, and freeze-dried at -80°C under vacuum for 3 h (Freeze dryer, SIM FD8-8T, SIM international, USA) then they were detached from the aluminum foil and stored in refrigerator (at 4°C) for further analysis.¹⁶ Blank NFs, as a control, was prepared with the same composition without CEO loading.

Characterization of CEO-NE-Based NFs

Scanning Electron Microscopy (SEM)

The surface morphology of electrospun CEO-NE-based NFs was observed with a scanning electron microscope (SEM) (JSM 6150, JEOL, Tokyo, Japan) operated at an accelerating voltage of 20 kV. SEM analysis was performed on a thin piece of NFs sheared from the center, using a sharp razor blade, and placed on double-sided adhesive tape onto the aluminum SEM stubs. It was made electrically conductive by coating with a thin layer of gold using a sputter gold coater (Sputter Coating Evaporator, SPI Module-Sputter Carbon/Gold Coater, USA) for 60 s to reduce electron charging effects. The average diameters of the individual fibers were measured using image J analysis software (NIH, USA).

Drug Content

The total amount of CEO loaded was evaluated by using freeze-dried CEO-NE-based NFs and its blank. After freeze-drying, 20 mg of the NFs mats were dissolved in 8 mL 1% (v/v) acetic acid using an ultrasonic bath (Sonix USA, SS101H230) for 1 h. One milliliter absolute ethanol was added to the medicated and blank solutions and the final volume was adjusted to 10 mL in volumetric flasks using 1% (v/v) acetic acid. The amount of CEO present in the obtained clear solution was quantified at 279 nm spectrophotometrically, utilizing double beam UV-VIS spectrophotometer (Labomed Inc., USA), using the solution from blank NFs.¹¹ The experiment was performed in triplicate and drug content was calculated as mean \pm SD.

Fourier-Transform Infrared Spectroscopy (FT-IR)

Characterization of pure PVA, freeze-dried CEO-NE-based NFs mat and its blank one were conducted using

Mattson 5000 FT-IR spectrophotometer (Madison Instruments, Middleton, Wisconsin, USA) at room temperature via potassium bromide (KBr) pellet technique. In total, the scanning range was 500 to 4000 cm^{-1} .

Differential Scanning Calorimetry (DSC)

DSC was implemented for thermal characterization of CEO-NE-based NFs using a Perkin-Elmer differential scanning calorimeter (DSC 6000, Waltham, MA, USA). Indium was utilized for the calibration process with purity and melting point of 99.99% and 156.6°C, respectively. Samples of each of CEO, medicated CEO-NE and its blank, pure PVA, freeze-dried CEO-NE-based NFs mat as well as its blank were crimped in standard aluminum pans and heated from 35°C to 350°C at a heating rate of 10°C/min under constant purging of dry nitrogen at 20 mL/min.

CEO-NE-based NEG as well as CEO-NE-based NFs were further appraised with respect to ex vivo permeation, kinetic analysis, and stability for a period of 6 months at refrigeration ($5 \pm 3^\circ\text{C}$) and ambient conditions. Finally, in vivo anti-inflammatory activity of the aforementioned medicated formulae against croton oil-induced mouse skin inflammation model in comparison with that of the corresponding plain ones and pure CEO was investigated. Assessments regarding histopathological examination and immunohistochemical (IHC) detection of cyclooxygenase-2 (COX-2) expression level were implemented. As well, the safety profile of CEO-NE-based NEG and CEO-NE-based NFs was evaluated by skin irritation test.

Ex vivo Skin Permeation Study

Skin Permeation Experiment

All animal experiments and skin samples preparations throughout the ex vivo and in vivo studies were accomplished after endorsement from the Scientific Committee of the Faculty of Pharmacy, Mansoura University, Egypt, in agreement with the Principles of Laboratory Animal Care NIH publication, 1985 revision (Code number: 2015–5).

Before carrying out the ex vivo permeation experiment, an animal hair clipper was used to remove the abdominal hair of newborn Wistar albino rats (2 weeks old). After 24 h, the skin was carefully inspected visually for its integrity. Then, the animals were sacrificed and their abdominal skin was excised with subsequent elimination of the visceral debris and adhering fat. Ultimately, the skin was wholly rinsed with distilled water and soaked overnight in an isotonic solution

(0.9% NaCl) at a refrigerator temperature, before the experiment. Locally fabricated Franz diffusion cells having donor and receptor compartments in a shaking incubator (GFL Gesellschaft für Labortechnik, Burgwedel, Germany) at $37 \pm 0.5^\circ\text{C}$ was used. A comparative study for drug diffusion and permeation from the topical formulations NEG and NFs matrices was assessed.

The excised rat skin was mounted on the donor half-cell, having a diameter of 1.5 cm and a surface area of 1.767 cm^2 , with the stratum corneum (SC) side faced the donor, whilst the dermal side was toward the receptor compartment. CEO in phosphate buffer, pH 7.4 (~2.33 mg/mL), CEO-NE-based NEG or CEO-NE-based NFs mat, containing the same amount of CEO, was introduced in the donor compartment and the receptor compartment was filled with 10 mL phosphate buffer, pH 7.4 and shaken at 75 rpm.

At predetermined intervals, 0.5, 1, 2, 3, 4, 5, 6, 7, 8, 24, 30 and 48 h, withdrawal of aliquots from the receptor medium was carried out followed by replenishing with an equivalent volume of fresh medium in order to conserve sink condition during the experiment. The collected aliquots were filtered by 0.45 μm millipore filter (Berlin, Germany) and analyzed for drug amount using a double beam UV-VIS spectrophotometer (Labomed Inc., USA) at 279 nm. The same protocol was implemented utilizing plain formulae corresponding to each of the investigated medicated ones as blank to abolish any interference arising from rat skin and formulae components.

Skin Permeation Parameters

The cumulative amount of CEO permeated the Wistar albino rats skin per unit area in the receiver chamber (Q , $\mu\text{g}/\text{cm}^2$) was plotted as a function of time (t , h) for the prepared CEO-NE-based NEG, CEO-NE-based NFs and pure CEO. The skin permeation parameters, namely, the cumulative amount of CEO permeating the Wistar albino rats skin after 48 h per unit area ($Q_{48\text{h}}$, $\mu\text{g}/\text{cm}^2$), steady-state flux (J_{ss} , $\mu\text{g}/\text{cm}^2\cdot\text{h}$), permeability coefficient (K_p) (cm/h), and enhancement ratio of flux (ER_{flux}) were calculated as reported.^{17,18}

Kinetic Analysis of Drug Permeation Data

To describe the mechanism of CEO permeation through the Wistar albino rats skin from the prepared CEO-NE-based NEG, CEO-NE-based NFs as well as pure CEO; the data obtained from the ex vivo permeation study were analyzed using different kinetic models. Three kinetic models which include zero-order, first-order, and Higuchi's square root models were

applied to the data.^{17,19} To assess the proper drug release mechanism, the data of the first 60% permeation were applied in Korsmeyer-Peppas model as follows (Equation 4):²⁰

$$\frac{M_t}{M_\infty} = Kt^n \quad (4)$$

where M_t/M_∞ , K and n are the fraction of drug released after time t , the release rate constant and the characteristic release exponent, respectively. The (n) value is used to characterize different release mechanisms. For example, (n) values of less than or equal to 0.5 are characteristic of Fickian or quasi-Fickian diffusion, whereas (n) values in the range of 0.5 to 1 are an indication of the anomalous drug release mechanism. It is worthy of note that the drug fractional release (M_t/M_∞) mechanism seems to be zero-order as n equals unity. The mathematical model that represented the best kinetic release profile was picked based on the highest coefficient of determination (R^2).

Stability Study

The prepared CEO-NE-based NEG was subjected to stability study as per International Conference for Harmonization (ICH) guidelines. A freshly prepared NEG formula was packaged in glass bottles and subjected to stability study under different storage conditions, namely; refrigeration ($5 \pm 3^\circ\text{C}$) and ambient conditions over a period of 6 months. Physical assessment of the samples was achieved by visual inspection of any phase separation, change in color and/or odor. Furthermore, the stability of CEO-NE-based NEG was assessed in terms of drug retention % and pH measurement at zero time (freshly prepared medicated NEG at production day), and after storage periods of 1, 2, 3, 4, 5 and 6 months. Its η was also determined at a rotational speed of 32 rpm (γ of 192 s^{-1}) at the designated periods of storage.^{14,21} Regarding CEO-NE-based NFs formulation, its stability was evaluated with respect to drug retention % periodically throughout 6-month period of storage in refrigerator ($5 \pm 3^\circ\text{C}$).

In vivo Assessment Studies

Animals

Male Swiss albino mice weighing 20–25 g were employed for the forthcoming in vivo anti-inflammatory activity and skin irritation experiments. The animals were caged and maintained for a one-week acclimatization period prior to conducting the experiments under standard laboratory conditions of $25 \pm 1^\circ\text{C}$ temperature, $55 \pm 5\%$ relative humidity (RH), and 12-h light/12-h dark photoperiod cycles with free

access to commercial laboratory chow and water ad libitum. Hair of the mice dorsal surface was depilated utilizing an animal hair clipper 1 day before executing the studies.

In vivo Anti-Inflammatory Activity Against Croton Oil-Induced Mouse Skin Inflammation Model

The anti-inflammatory activity of the investigated formulae was assessed employing the documented croton oil-induced skin inflammation model.²² The mice were divided into eight groups (6 animals per group), totaling a final number of 48 animals and served as follows:

- Group A: Normal control (no croton oil nor CEO).
- Group B: Croton oil (once topical application of single dose of 8 mg croton oil/0.2 mL acetone and left for 24 h). These conditions (dose and time) provoked maximum inflammatory response as previously reported.²²
- Group C: Pure CEO (once topical treatment/day with 1 μL of CEO after 24 h of croton oil application).
- Group D: CEO-NE-based NEG (once topical treatment/day with 0.6 g NEG (1% w/w CEO) after 24 h of croton oil application).
- Group E: Plain-NE-based NEG (twice topical treatment/day (every 12 h) with 0.6 g NEG (without CEO) after 24 h of croton oil application).
- Group F: CEO-NE-based NEG (twice topical treatment/day (every 12 h) with 0.6 g NEG (1% w/w CEO) after 24 h of croton oil application).
- Group G: Plain-NE-based NFs (once topical treatment/day with 100 mg NFs (without CEO) after 24 h of croton oil application).
- Group H: CEO-NE-based NFs (once topical treatment/day with 100 mg NFs (1% w/w CEO) after 24 h of croton oil application).

Plain and medicated NEG and NFs were prepared as previously mentioned. Such formulae were applied to the mice's dorsum and covered by Tegaderm (3M Health Care, USA) and additionally secured firmly by specially designed mouseVelcro jackets.^{23,24} In the present study, pure CEO was topically applied for comparison. It was reported that the anti-inflammatory activity of NE containing eugenol, the main component of CEO, against carrageenan-induced paw edema model was proved with no significant difference in the concentration range of 1–4% (w/w).²⁵

Preparation of Skin Tissue Samples

The treatment regimen was continued for only 1 day. After that, the animals were sacrificed and dorsal skin tissue samples were excised, fixed in 10% buffered formalin solution, processed for paraffin wax embedding and sectioned into 5 μm thickness for the subsequent histopathological and IHC evaluations.

Histopathological Evaluation

One set of skin tissue sections was deparaffinized and stained with hematoxylin and eosin (H&E).²⁶ The intensity of the inflammatory response was assessed in six histological sections from each mouse per group. A minimum of 10 fields for each slide were examined (at 100 \times and 400 \times magnification) and scored. The degree of inflammation was evaluated with a score from 0 to 5. The scores were defined as follows: 0=no inflammation, 1=mild inflammation, 2=mild/moderate inflammation, 3=moderate inflammation, 4=moderate/severe inflammation and 5=severe inflammation.^{27,28}

IHC Evaluation of COX-2 Expression

Second set of sections was subjected to IHC evaluation of COX-2 expression level employing EnVision method according to the manufacturer's instructions as previously reported.²³ The level of IHC staining intensity was scored 0, negative; 1, weak; 2, moderate and 3, strong staining.²⁹

To abolish a source of bias, all the stained sections were examined under a light microscope (Olympus, Tokyo, Japan) and digital images were captured, and then evaluated by a qualified experienced pathologist blind to the experimental groups and treatments.

Skin Irritation Test

After shaving the hair of the dorsal side of the mice 24 h before starting the experiment, the animals were divided into four groups (six animals/group) as follows:

- Group I: Normal control without any treatment.
- Group II: Standard irritant (topical application of formalin aqueous solution (0.8% v/v)).²³
- Group III: CEO-NE-based NEG (twice topical application/day (every 12 h) with 0.6 g NEG (1% w/w CEO)).
- Group IV: CEO-NE-based NFs (once topical application/day with 100 mg NFs (1% w/w CEO)).

The same fixation method of the investigated formulae on the mice's dorsum was proceeded as mentioned above in the

"In vivo anti-inflammatory activity" section. The protocol of skin irritation test was continued for only 1 day followed by sacrificing the mice and dissecting the treated skin tissues for histopathological examination after (H&E) staining utilizing a light microscope (Olympus, Tokyo, Japan).

Statistical Analysis

The ex vivo and stability data were statistically analyzed using ANOVA followed by Tukey–Kramer multiple comparisons test except for ER_{flux} that was analyzed by Student's *t*-test (unpaired *t*-test) and expressed as mean \pm SD. In case of in vivo study, Kruskal–Wallis test (non-parametric test) was applied followed by Dunn multiple comparison test for statistical analysis of both the inflammatory and IHC scores.³⁰ GraphPad Prism 5 application software was employed for the analysis process. The statistical significant differences were considered at $p < 0.05$.

Results and Discussion

Characterization of CEO-NE Formula Physical Characterization

CEO-NE formula passed thermodynamic stability as well as self-nanoemulsification efficiency tests. It was found to have a negative ZP charge (-14.60 ± 2.34), a nanometric size (81.53 ± 11.15 nm) and a low PDI value (0.245 ± 0.04). Additionally, the prepared formula expressed high %T value of $100.38 \pm 0.75\%$, drug content (%) of $96.62 \pm 1.78\%$ as well as acceptable η (33.28 ± 7.84 cP) and pH (4.01 ± 0.07).

Fourier-Transform Infrared Spectroscopy (FT-IR)

Figure 2A shows the FT-IR spectra of native CEO, GMA, Labrasol and tween 80[®]. As a comparison, the FT-IR spectra of CEO: GMA dilution (in a ratio of 1:8), CEO-NE and its blank are illustrated, as well.

CEO spectrum (a) exhibited signature peaks at 3523, 3071 and 2934 cm^{-1} assigned to O-H, =C-H, and C-H stretching, respectively. As well, sharp peaks at 1609 and 1514 cm^{-1} originated from C=C stretching of the aromatic moiety, whereas the peak at 1269 cm^{-1} pointed out to C-O stretching.^{11,31}

For GMA (b), signals at 1731 and 1377 cm^{-1} from the carbonyl (C=O) stretch of the ester and alcohols (OH), respectively, were observed. Additionally, characteristic (C-H alkane stretch) signals were noticed at 2953 and 2890 cm^{-1} , while a distinguished band of OH was recorded at 3406 cm^{-1} .^{32,33}

The infrared spectrum of Labrasol (c) showed broad peaks nearly at 3040–3600 (3416) cm^{-1} (O-H stretch),

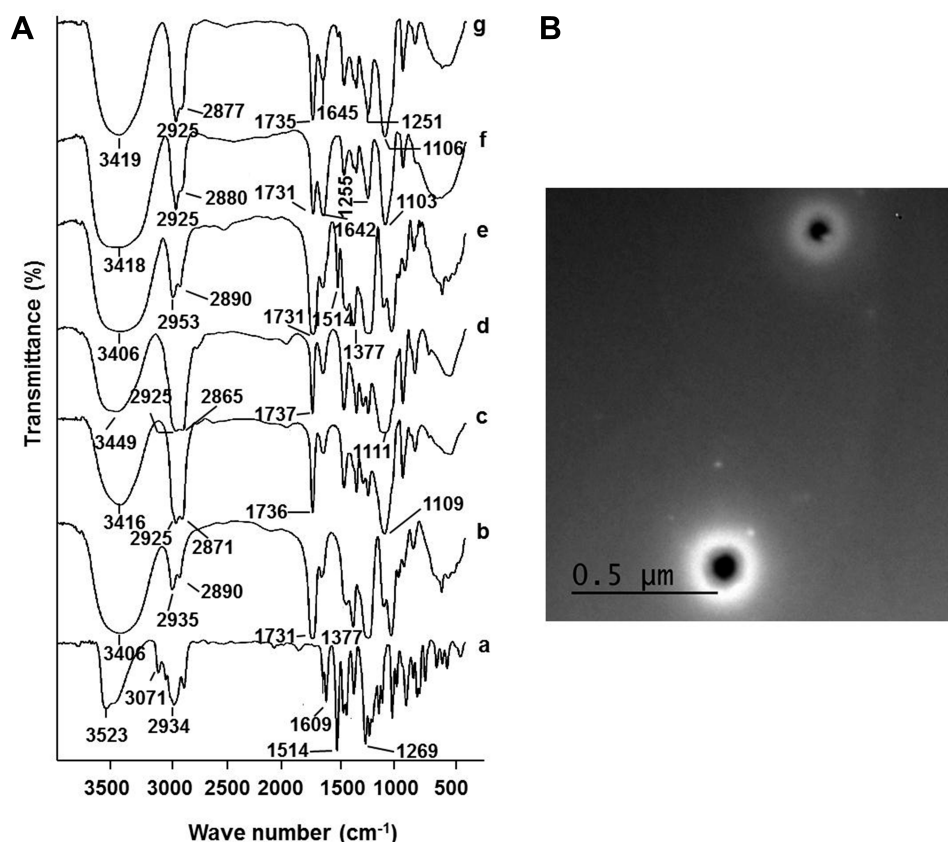


Figure 2 FT-IR spectra of NE and its individual components (**A**) and TEM image of CEO-NE (**B**).

Notes: FT-IR spectra of pure CEO (a), GMA (b), Labrasol (c), tween-80[®] (d), CEO: GMA dilution (in a ratio of 1:8) (e), blank NE (f), and CEO-NE (g).

Abbreviations: CEO, clove essential oil; FT-IR, Fourier transform infrared spectroscopy; GMA, glycerol monoacetate; NE, nanoemulsion; TEM, transmission electron microscope.

distinctive sharp peaks at 2925 and 2871 cm^{-1} (C-H stretch) and at 1736 cm^{-1} (C=O stretch) as well as broad peaks at approximately 1200–1000 (1109) cm^{-1} (C-O stretching).³⁴

FT-IR spectrum of tween-80[®] (d) displayed numerous sharp and intense peaks due to the presence of different functional groups. The strong band around 3449 cm^{-1} could be related to the O-H stretching vibrations. The bands centered at 2925 and 2865 cm^{-1} were associated with methyl (-CH₃) group absorption band and methylene (-CH₂) group stretching vibrations, respectively. The band at 1737 cm^{-1} could be attributed to C=O stretching of the ester group, while the band at 1111 cm^{-1} referred to stretching of C-O-C.³⁵

The FT-IR spectrum of CEO: GMA dilution, in a ratio of 1:8, (e) disclosed the peaks of CEO along with that of GMA. The characteristic peaks of GMA (1731, 1377, 2953, 2890 and 3406 cm^{-1}) were predominant, probably due to the dilution effect.

Peaks in blank NE (3418, 2925, 2880, 1731, 1642, 1103 cm^{-1}) were related to some peaks in GMA, Labrasol,

tween-80[®], with a minor shift. This might indicate the occurrence of some interactions between NE components and water, causing a shift and broadening of the peaks, as depicted in (f).³⁶ CEO-NE peaks (g) elicited the same peaks of its blank indicating no interaction.

Transmission Electron Microscopy (TEM)

TEM analysis has been one of the most accomplished assessment for identifying the morphology, structure and particle size frequency. Figure 2B shows homogeneous and spherical droplets of CEO-NE. It is known that NE with spherical morphology can disperse well without aggregation.³⁷

Physicochemical Characterization and Optimization of the Prepared Blank Hydrogels

Taguchi's Design of the Experiment

Signal-to-Noise Ratio ((S/N) Ratio)

The average value of the (S/N) ratio, expressed in decibel (dB), at different levels of ICPs for mean pH and mean η

at γ of 192 s^{-1} are illustrated as (S/N) graphs in Figure 3A and B, respectively. Basically, it is defined in the model that larger (S/N) ratio is the optimized quality characteristic for the prepared hydrogels and in turn will be essential for determining the optimum levels of ICPs.

The L9 OA response values for DMPs and the corresponding (S/N) ratios are shown in Table 3. F-9 experienced the highest mean η at γ of 192 s^{-1} as well as the highest mean (S/N) ratio. Meanwhile, the mean (S/N) ratio for every level of the three ICPs is summarized and demonstrated in Table 4. As shown in Table 4, the delta value of ((maximum–minimum) (S/N) ratios) of CS concentration (X_1) is the highest value for both tested DMPs. Hence, it can be concluded that CS concentration (X_1) is the most important one affecting both the tested DMPs.³⁸

ANOVA

The purpose of ANOVA, which is a statistically based objective decision-making tool, is to investigate which ICPs significantly affected the DMPs of the prepared hydrogels. Figure 4 shows the contribution (%) of CS concentration (X_1) which has the highest significant effect on the prepared hydrogels' performance indicators; pH as well as η at γ of 192 s^{-1} . A profound look at ANOVA data (Figure 4) demonstrated the discrepancy in the contribution (%) of GG and GA in both tested DMPs. For instance, GG contribution (%) was higher than that of GA in case of η measurement and vice versa in pH data. It should be kept in consideration that the η is the vital DMPs as its values were greatly influenced by the ICPs attested while pH measurements were in the acceptable range in all the

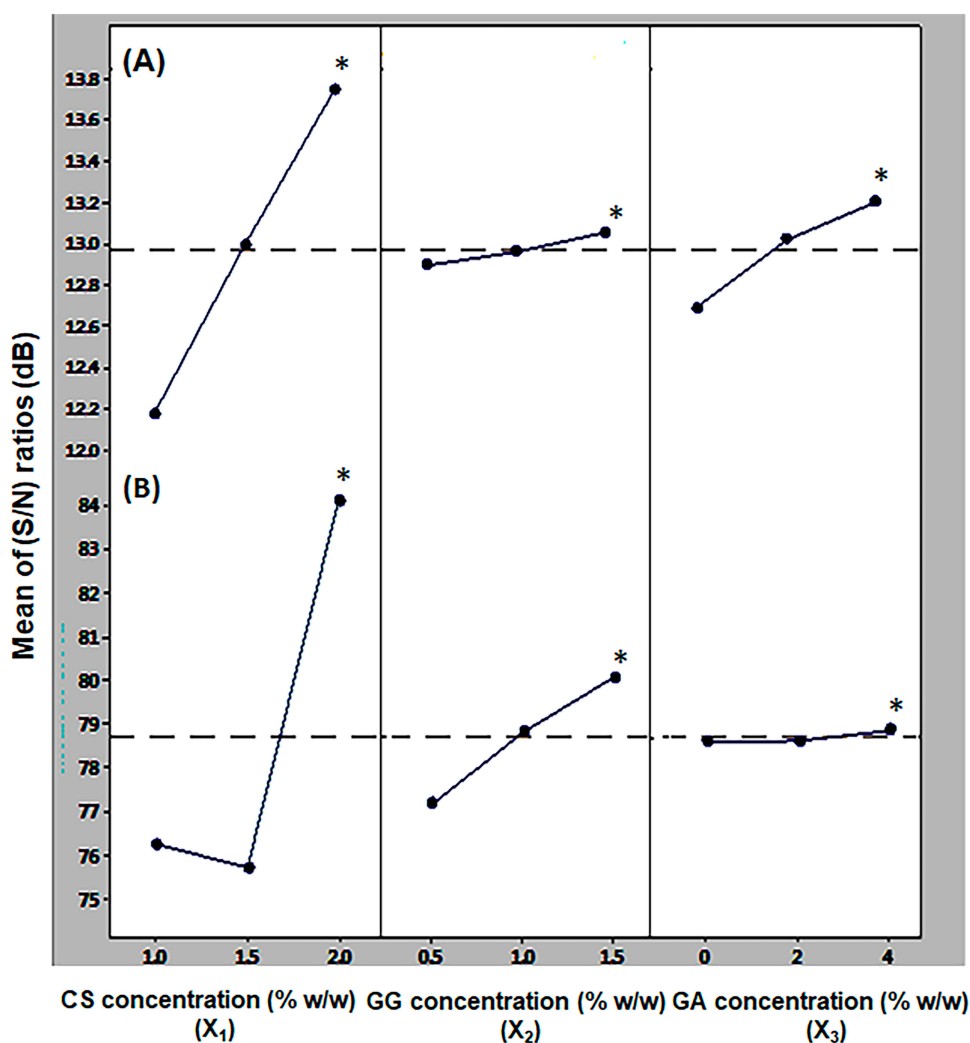


Figure 3 Graphs illustrating the mean (S/N) ratios of the DMPs against the concentration of the different ICPs.

Notes: ((A) mean pH, and (B) mean η at γ of 192 s^{-1}) See Table 4. *Points to the highest values.

Abbreviations: (S/N), signal-to-noise ratio; DMPs, dependently measured parameters; ICPs; independently controlled parameters; η , viscosity; γ , shear rate.

Table 3 Taguchi L9 OA Response Values and (S/N) Ratios for DMPs of the Prepared Blank Hydrogels (See Tables 1 and 2)

Formula No.	Mean pH*	(S/N) Ratio for Mean pH	Mean η (cP) at γ of 192 s^{-1} *	(S/N) Ratio for Mean η at γ of 192 s^{-1}
F-1	3.87 \pm 0.01	11.75	5214.06 \pm 156.89	74.34
F-2	4.09 \pm 0.05	12.23	6767.19 \pm 156.89	76.61
F-3	4.23 \pm 0.03	12.53	7765.62 \pm 313.78	77.80
F-4	4.47 \pm 0.02	13.01	5103.12 \pm 313.78	74.16
F-5	4.55 \pm 0.03	13.16	6101.56 \pm 470.67	75.71
F-6	4.37 \pm 0.04	12.81	7321.87 \pm 313.78	77.29
F-7	4.97 \pm 0.04	13.93	14,200.00 \pm 1568.89	83.04
F-8	4.73 \pm 0.05	13.50	16,085.94 \pm 1412.01	84.13
F-9	4.91 \pm 0.02	13.82	17,971.88 \pm 313.78	85.09

Notes: *Each value represents the mean \pm SD (n=3).

Abbreviations: cP, centipoise; DMPs, dependently measured parameters; OA, orthogonal array; (S/N), signal-to-noise ratio; η , viscosity; γ , shear rate.

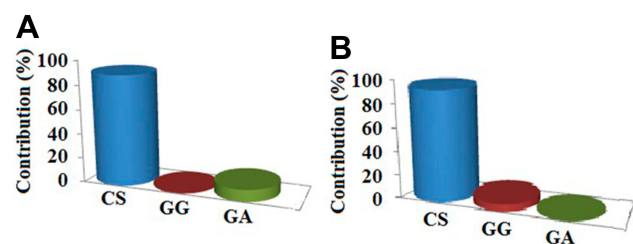
Table 4 Computer Calculated (S/N) Ratios for the Tested DMPs (A) Mean pH and (B) Mean η at γ of 192 S^{-1} (cP) with Regard to the Different ICPs (See Table 1)

(A)				(B)			
Level	CS Concentration	GG Concentration	GA Concentration	Level	CS concentration	GG concentration	GA concentration
1	12.17	12.90	12.69	1	76.25	77.18	78.59
2	12.99	12.96	13.02	2	75.72	78.82	78.62
3	13.75	13.05	13.20	3	84.09	80.06	78.85
Delta	1.58	0.16	0.52	Delta	8.37	2.88	0.26
Rank	1	3	2	Rank	1	2	3

Notes: Delta = (maximum–minimum) (S/N) ratios. Rank according to the value of delta.

Abbreviations: cP, centipoise; CS, chitosan; DMPs, dependently measured parameters; GA, gum acacia; GG, guar gum; ICPs, independently controlled parameters; (S/N), signal-to-noise ratio; η , viscosity; γ , shear rate.

prepared formulae (Table 3). Consequently, GG represents the secondary effective ICPs following CS compared to GA. Based on the above-mentioned data, it can be deduced that CS concentration (X_1) is the most pivotal parameter affecting the tested DMPs. Such conclusion coincides with that obtained from the (S/N) ratio response table (Table 4).

**Figure 4** Results of ANOVA for contribution (%) of each factor on the performance characteristics.

Notes: (A) pH and (B) η at γ of 192 s^{-1} .

Abbreviations: ANOVA, analysis of variance; η , viscosity; γ , shear rate.

Physicochemical Characterization of the Prepared Blank Hydrogels

Visual Examination

Results of the visual inspection of the blank hydrogels demonstrated that all of the prepared blank hydrogels were either yellow transparent or off-white translucent in color. All of them showed very good homogeneity, smooth homogenous texture with a lack of lumps and/or syneresis. No indications of grittiness, as well.

pH Determination

pH values of the prepared blank hydrogels were in the range of 3.87 ± 0.01 to 4.97 ± 0.04 . The increment of CS concentration (X_1) increases the number of free amino groups that may undergo protonation, thus remarkably reducing the number of free protons and increasing pH values as shown in Table 3. Such manner matches the results obtained from both (S/N) ratio response (Table 4) and ANOVA results (Figure 4) which approved that CS concentration (X_1) is the most important parameter affecting pH value. The formulations containing CS (2% w/w)

exhibited the highest pH values ranged from 4.73 ± 0.05 to 4.97 ± 0.04 (Tables 2 and 3), which are suitable for topical application.^{39,40}

Rheological Study

CS and GG are known to exhibit pseudoplastic or shear-thinning behavior in aqueous solutions which refers to a decrease in η with increasing $\dot{\gamma}$.^{41,42} F-9, having both CS and GG concentrations at their highest level, level 3, and GA concentration at its medium level, level 2 (Table 2), disclosed the highest η amongst all the prepared blank hydrogels at $\dot{\gamma}$ of 192 s^{-1} (Figure 5 and Table 3).

Since F-9 experienced the highest η and acceptable pH of 4.91 ± 0.02 , which are suitable for skin application, it was selected for further elaborate formulation into CEO-NE-based NEG.

Characterization of the Prepared CEO-NE-Based NEG

Visual Examination

CEO-NE-based NEG was homogenous, yellow and transparent as well as free from any turbidity or grittiness.

pH Determination

CEO-NE-based NEG has pH value of 4.51 ± 0.01 , which is suitable for topical application.^{39,40}

Measurement of Viscosity

The measured η of the prepared CEO-NE-based NEG was $6545.31 \pm 156.89 \text{ cP}$ which will be acceptable for topical application.¹⁸

Assay of Drug Content

Drug content for the prepared CEO-NE-based NEG was found to be $99.350 \pm 1.672\%$.

Fourier-Transform Infrared Spectroscopy (FT-IR)

Figure 6A shows the FT-IR spectra of native CS, GG, GA and their physical mixture corresponding to the optimized formula (F-9). As a comparison, the FT-IR spectra of CEO-NE-based NEG and its blank are depicted, as well.

A typical characteristic polysaccharide absorption bands at 3447 and 3422 cm^{-1} ($-\text{OH}$ groups stretching) were obvious in the spectra of the three used polymers CS, GG and GA (a, b and c). Similarly, the aforementioned spectra possess peaks at $3000\text{--}2800$ and 1651 cm^{-1} which stand for aliphatic groups ($-\text{CH}_2$ and $-\text{CH}_3$) and carbonyl group ($-\text{C}=\text{O}$) stretching vibrations, respectively.

On the other hand, in the range of $800\text{--}1500 \text{ cm}^{-1}$, CS (a) shows several peaks. The peaks at 1425 and 1340 cm^{-1} represent oscillations characteristic for $-\text{OH}$ and C-H bending of CH_2 groups, respectively. The peak at 1381 cm^{-1} is related to the C-O stretching of the primary alcoholic group ($-\text{CH}_2\text{-OH}$). Additionally, the broad peak at $1154\text{--}1031 \text{ cm}^{-1}$ represents the bridge $-\text{O}-$ stretch of the glucosamine residues.^{43,44}

In case of GG (b), peak at 1007 cm^{-1} and the region around 1400 cm^{-1} were due to O-H bending vibrations and CH_2 deformation, respectively.^{45,46} Additionally, pure GA spectrum (c) shows different peaks at 1426 cm^{-1} (O-H bending of acid group), 1072 cm^{-1} (C-O stretching) and 1030 cm^{-1} (O-H bending).⁴⁷

FT-IR spectrum of the polymers physical mixture (d) showed neither disappearance of existed peaks nor appearance of extra peaks, thereby establishing the absence of physical interaction between the polymers at the used ratio.

FT-IR spectra of the blank NEG and CEO-NE-based NEG (e and f) elucidate the peaks of blank NE and/or that of CEO-NE (as depicted in Figure 2A(f and g)) along with

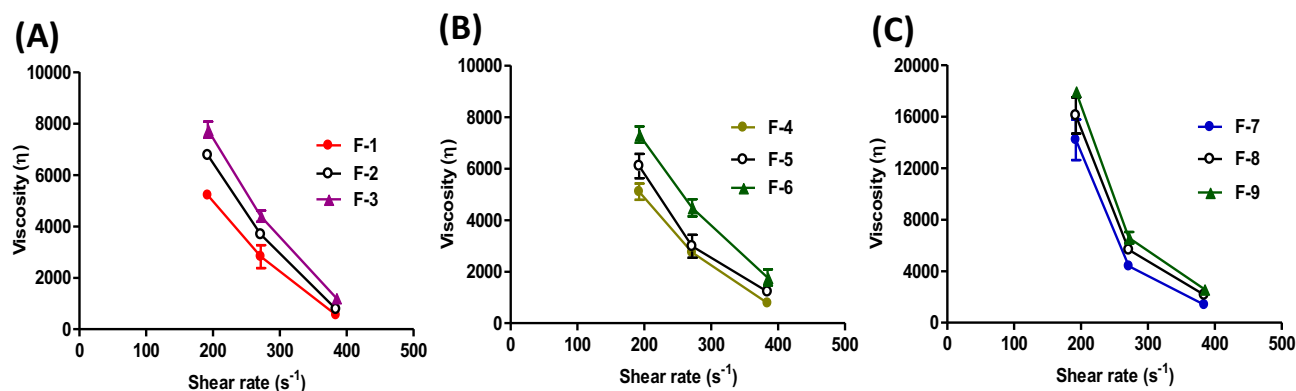


Figure 5 Shear thinning behavior of the prepared blank hydrogels with F-9 having the highest η .

Notes: (A) F-1–F-3, (B) F-4–F-6 and (C) F-7–F-9.

Abbreviation: η , viscosity.

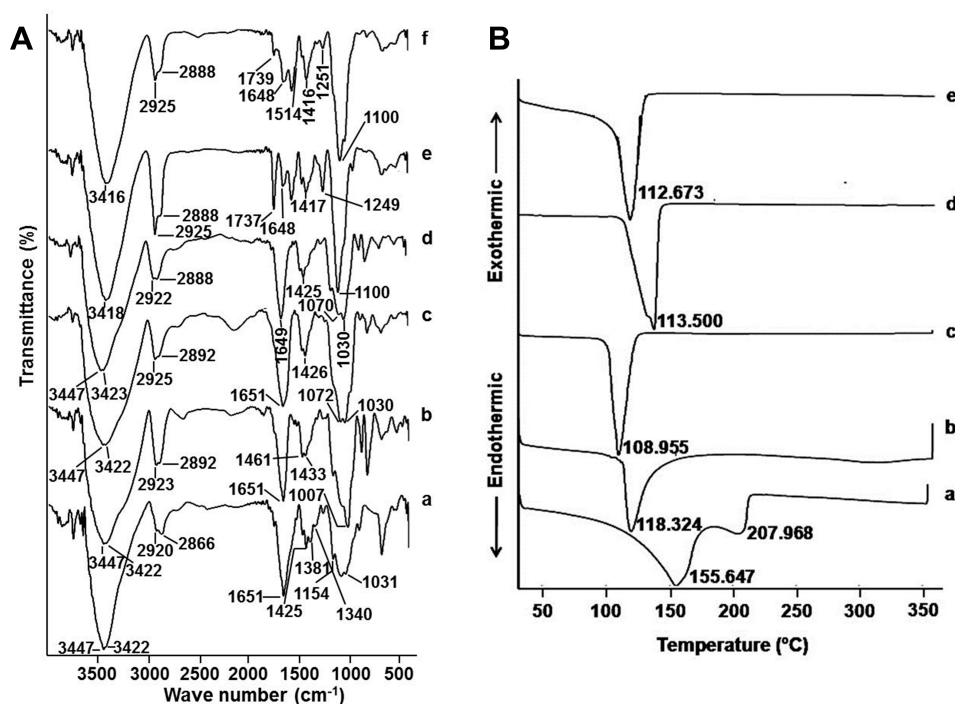


Figure 6 FT-IR spectra and DSC of NEG and its individual components.

Notes: (A) FT-IR spectra of pure CS (a), GG (b), GA (c), physical mixture of the optimized formula (F-9) (d), blank NEG (e), CEO-NE-based NEG (f) and (B) DSC of pure CEO (a), blank NE (b), CEO-NE (c), blank NEG (d), CEO-NE-based NEG (e).

Abbreviations: CEO, clove essential oil; CS, chitosan; DSC, differential scanning calorimetry; FT-IR, Fourier transform infrared spectroscopy; GA, gum acacia; GG, guar gum; NE, nanoemulsion; NEG, nanoemulgel.

the used polymers' characteristic peaks reflecting the molecular dispersion of NE either blank or medicated in the prepared NE-based NEG.

Differential Scanning Calorimetry (DSC)

DSC was accomplished to study the thermal behavior of the CEO in the prepared CEO-NE-based NEG, and the thermograms are depicted in Figure 6B. Pure CEO (a) showed well-defined endothermic events, at 155.647°C and 207.968°C, attributed to the CEO boiling and evaporation processes.¹¹ In the thermograms of both blank NE and CEO-NE (b and c, respectively), an endothermic peak was observed around 100°C, most probably due to water evaporation. Such behavior suggests that CEO was molecularly dispersed in the oil phase of the NE.⁴⁸ Likewise, the same behavior was noticed in the thermograms of both blank NEG and CEO-NE-based NEG (d and e) revealing the molecular dispersion of CEO in the prepared NEG.⁴⁹

Characterization of CEO-NE-Based NFs

Scanning Electron Microscopy (SEM)

The SEM image and the diameter distribution histogram of the CEO-NE-based NFs mats are illustrated in Figure 7. This image revealed bead-free and smooth NFs without

phase separation of the NE from the NFs mats. The average diameters of the CEO-NE-based NFs were 306.4 ± 92.1 nm.

Drug Content

The amount of CEO was found to be 1.00 ± 0.03 mg CEO loaded in 100 mg CEO-NE-based NFs (drug entrapment efficiency percentage (DEE%) = $40.02 \pm 1.15\%$).

Fourier-Transform Infrared Spectroscopy (FT-IR)

The FT-IR spectra of pure PVA, as well as freeze-dried mats of blank and CEO-NE-based NFs are shown in Figure 8A. All major peaks pertained to hydroxyl and acetate groups (residue from saponification reaction of polyvinyl acetate) were observed in the FT-IR spectrum of PVA (a). More particularly, the broadband inspected between 3681 and 3129 cm⁻¹ is correlated to the O-H stretch from the intermolecular and intramolecular hydrogen bonds. The vibrational peak observed between 2860 and 2987 cm⁻¹ is the outcome of the C-H stretch from alkyl groups. The bands between 1773 and 1702 cm⁻¹ are owing to the C=O stretching, from the existing acetate groups in PVA, while that at 1650 cm⁻¹

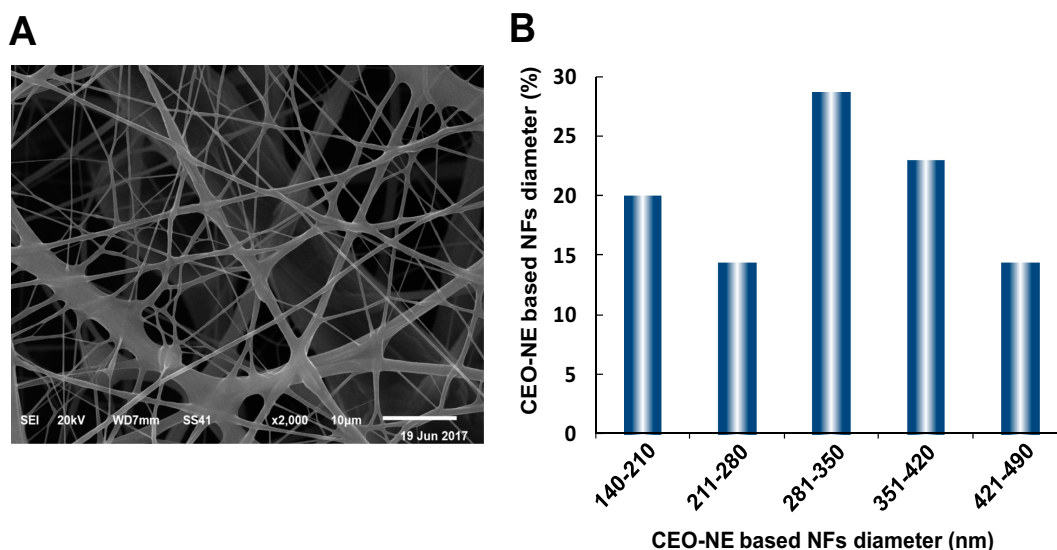


Figure 7 SEM image (A) and diameter distribution histogram (B) of CEO-NE-based NFs.
Abbreviations: CEO, clove essential oil; NE; nanoemulsion; NFs, nanofibers; SEM, scanning electron microscopy.

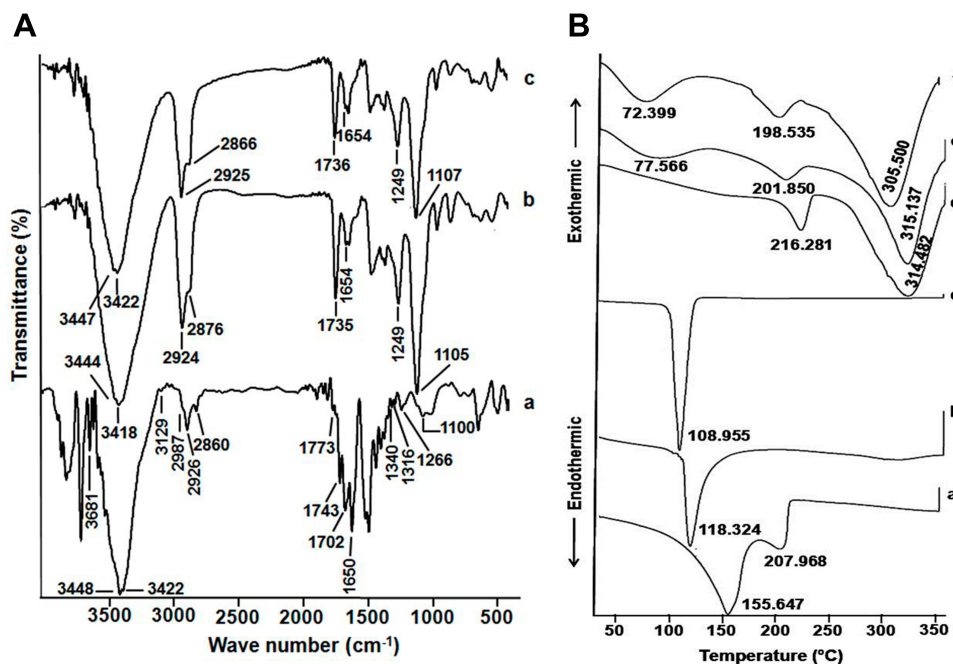


Figure 8 FT-IR spectra and DSC of NFs and their individual components.

Notes: (A) FT-IR spectra of pure PVA (a), blank NFs (b), CEO-NE-based NFs (c) and (B) DSC of pure CEO (a), blank NE (b), CEO-NE (c), PVA (d), blank NFs (e), CEO-NE-based NFs (f).

Abbreviations: CEO, clove essential oil; DSC, differential scanning calorimetry; FT-IR, Fourier transform infrared spectroscopy; NE, nanoemulsion; NFs, nanofibers; PVA, polyvinyl alcohol.

is due to O-H bending (water absorption band). Additionally, the peaks at 1340 and 1316 cm^{-1} are due to C-H bending, while those at 1266 and 1100 cm^{-1} correspond to C=O vibration and C-O stretching in the C-O-H group, respectively.^{50,51}

The spectra of blank NFs and CEO-NE-based NFs mats (b and c) showed all features of the peaks that were displayed in the spectra of both CEO-NE and its blank (as elucidated in Figure 2A(f and g)) along with PVA characteristic peaks. It seems to be the evidence for the

complete dispersion of the CEO-NE into the PVA polymer matrix.

Differential Scanning Calorimetry (DSC)

DSC studies were accomplished to probe the thermal behavior of the CEO in the electrospun NFs mats, and the thermograms are displayed in Figure 8B. Pure CEO, blank NE and CEO-NE peaks (a, b and c) were discussed previously (in DSC of CEO-NE-based NEG).

Additionally, the DSC of PVA (d) shows two melting endothermic peaks at 216.281°C and 314.482°C.⁵² The thermograms of the blank NFs and CEO-NE-based NFs mats (e and f) are quite similar, where they show a broad endothermic peak corresponding to dehydration at 77.566°C and 72.399, respectively. Besides, the two peaks of PVA melting show minor shift compared to that of the pure PVA thermogram. This DSC data clarify that CEO is molecularly dispersed into the PVA-NFs matrix, which matches FT-IR data.

Ex vivo Skin Permeation Study

Skin Permeation Experiment and Parameters

As illustrated in Figure 9, the ex vivo permeation outlines of CEO from the prepared CEO-NE-based NEG and CEO-NE-based NFs through the excised Wistar albino rats' skin were different from that of the control (pure CEO). According to the calculated Q_{48h} , the permeation rate was in the order of CEO-NE-based NEG > CEO-NE-based NFs > pure CEO.

CEO-NE-based NEG showed the highest permeation efficiency compared to CEO-NE-based NFs as well as pure CEO. It is known that NEG influences a better skin

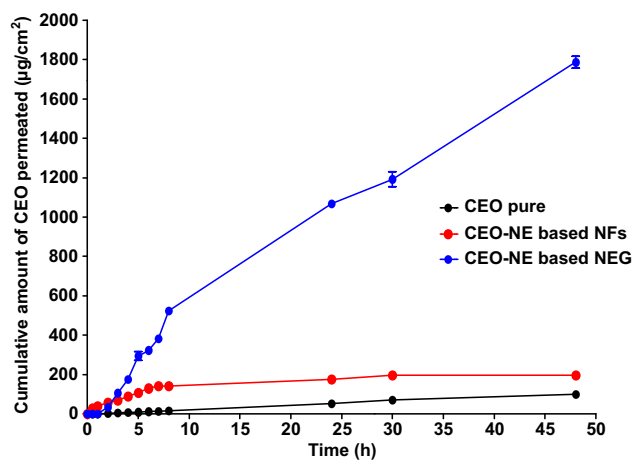


Figure 9 Ex vivo skin permeation profiles of CEO from pure CEO, CEO-NE-based NFs and CEO-NE-based NEG.

Notes: Each point represents the mean \pm SD (n=3).

Abbreviations: CEO, clove essential oil; NE, nanoemulsion; NEG, nanoemulgel; NFs, nanofibers.

permeation owing to the characteristics of the gel polymeric matrix as follows: 1) good adhesion property particularly the positively charged CS that can bind to the negatively charged skin at physiological pH condition through electrostatic interaction; and 2) penetration enhancement ability of CS when applied topically. These characteristics facilitate the controlled release of the medicated NE particles from the gel matrix, hence allowing their penetration into the SC of the skin.⁵³

On the other hand, it can be seen that CEO-NE-based NFs' permeation across the skin was gradual. Such behavior could be explained on the basis of the low degradation rate of PVA NFs, which could increase the opportunity for drug deposition and retention in the skin and subsequently sustain its permeation.⁵⁴

Regardless of the effect of polymeric matrix type in both investigated systems (NEG and NFs), the influence of the NE system on the permeation of the loaded drug should be also kept into consideration. The NE's nano-size and penetration-enhancing capability related to its component (surfactant; tween-80[®]) greatly support and augment the drug permeation through the skin. Additionally, the high solubilization of the drug conferred by loading into the NE system leads to larger concentration gradient towards the skin which further increases skin permeation of drug.¹⁸

As depicted in Table 5, it could be inferred that CEO-NE-based NFs as well as CEO-NE-based NEG formulations shows a significant difference ($p < 0.05$) as for all the permeation parameters vs each other as well as vs the control (pure CEO). Conspicuously, CEO-NE-based NEG exhibited the highest permeation parameters including Q_{48h} ($1786.61 \pm 29.14 \mu\text{g}/\text{cm}^2$), J_{ss} ($31.32 \pm 0.40 \mu\text{g}/\text{cm}^2\cdot\text{h}$), K_p ($13.44 \pm 0.00 \times 10^{-3} \text{ cm}/\text{h}$), and ER_{flux} (16.76 ± 0.74). Hence, it can be concluded that polymeric PVA NFs (ie CEO-NE-based NFs) can sustain the penetration of CEO through the skin, when compared to CEO-NE-based NEG, and help maintaining the effective CEO concentration in the skin for a prolonged period.⁵⁴

Kinetic Analysis of Drug Permeation Data

To inspect the mechanism of drug release, (R^2) and the release kinetic parameters were calculated for the investigated pure CEO, CEO-NE-based NFs and CEO-NE-based NEG (Table 6). It can be deduced from the (R^2) as well as (n) values that Higuchi's kinetic model as well as Fickian diffusion mechanism dominated for CEO-NE-based NFs permeation, which indicates that the release of CEO from

Table 5 Ex vivo Skin Permeation Parameters of CEO from Pure CEO, CEO-NE Based NFs and CEO-NE-Based NEG Across the Excised Wistar Albino Rats' Skin After 48 h

Formulation	Q _{48h} (µg/cm ²)	J _{ss} (µg/cm ² .h)	K _p (cm/h)×10 ⁻³	ER _{flux}
Pure CEO	99.97 ± 2.32	1.87 ± 0.06	0.80 ± 0.00	–
CEO-NE-based NFs	196.81 ± 0.36*	2.41 ± 0.12*	1.04 ± 0.00*	1.29 ± 0.10
CEO-NE-based NEG	1786.61 ± 29.14*#	31.32 ± 0.40*#	13.44 ± 0.00*#	16.76 ± 0.74**

Notes: Each value represents the mean ± SD (n=3). *Significant at $p < 0.05$ vs pure CEO using ANOVA. #Significant at $p < 0.05$ vs CEO-NE-based NFs using ANOVA. **Significant at $p < 0.05$ vs CEO-NE-based NFs using Student's *t*-test (unpaired *t*-test).

Abbreviations: CEO, clove essential oil; ER_{flux}, enhancement ratio of flux; J_{ss}, steady-state flux; K_p, permeability coefficient; NE, nanoemulsion; NEG, nanoemulgel; NFs, nanofibers, Q_{48h}, the cumulative amount of CEO permeating the Wistar albino rats skin after 48 h per unit area.

Table 6 Kinetic Analysis of the ex vivo Permeation Data of CEO from Pure CEO, CEO-NE-Based NFs and CEO-NE-Based NEG

Formula	Coefficients of Determination (R ²)			Korsmeyer-Peppas		
	Zero-Order	First-Order	Higuchi Model	(R ²)	Diffusional Exponent (n)	Main Transport Mechanism
Pure CEO	0.9946	0.9939	0.9255	0.9978	1.12	Super case II transport
CEO-NE-based NFs	0.6569	0.6745	0.8720	0.9235	0.45	Fickian
CEO-NE-based NEG	0.9619	0.9401	0.8148	0.9657	1.88	Super case II transport

Abbreviations: CEO, clove essential oil; NE, nanoemulsion; NEG, nanoemulgel; NFs, nanofibers.

polymeric PVA NFs (namely CEO-NE-based NFs) seems to be a process controlled mainly by diffusion.

Otherwise, a zero-order release pattern was observed for both pure CEO and CEO-NE-based NEG as estimated by (R²) and (n) values. Similar findings were previously reported when NE based hydrogel for enhanced transdermal delivery of ketoprofen and in situ NEG of quercetin for periodontitis were prepared.^{21,55}

The best fit of the zero-order model indicated that the drug release from the prepared NEG followed controlled-release pattern. Additionally, it is known that (n) value higher than unity (1) indicates super case II transport mechanism which results from swelling and polymer chain relaxation of polymeric-blend (CS-GG-GA) matrix.⁵⁶

Stability Study

One of the most important characteristics is the stability study of the developed formulation. In the present study, CEO-NE-based NEG did not display any phase separation or physical changes, in color and/or odor, over a storage period of 6 months at refrigeration conditions (5 ± 3°C) revealing its good stability. The samples have yellow color and transparent appearance free from any turbidity or grittiness. Such good stability of the NEG formulation may be attributed to the stability of the initial NE used in its preparation. Contrary, turbidity of CEO-NE-based NEG was noticed at the end of storage at ambient conditions.

Table 7 summarizes the values of drug retention %, pH and η at γ of 192 s⁻¹ of the prepared CEO-NE-based NEG stored at the two diverse conditions. The data of ANOVA clarified the insignificant variation in drug retention %, pH and η at γ of 192 s⁻¹ during the refrigerated storage periods. Otherwise, a significant increment in pH, as well as a decrement in drug retention % and η at γ of 192 s⁻¹ was recorded at ambient storage condition before the storage period termination.

Fortunately, for CEO-NE-based NFs, the value of drug retention % was found to be 97.74 ± 2.01 after 6 months storage at 5 ± 3°C.

Consequently, the obtained data displayed an obvious evidence of the stability of both CEO-NE-based NEG and CEO-NE-based NF_s formulae upon refrigerated storage condition (5 ± 3°C), therefor empowering their efficiency for prolonged extent. Electrospun eugenol/cyclodextrin inclusion complex nanofibrous mats were reported to be kept in refrigerator.¹⁶

In vivo Assessment Studies

In vivo Anti-Inflammatory Activity Against Croton Oil-Induced Mouse Skin Inflammation Model

Croton-oil induced skin inflammation is a well-established pharmacological model for screening the anti-inflammatory activity of the investigated drugs either free or incorporated in pharmaceutical delivery systems that

Table 7 Drug Retention %, pH, and η at γ of 192 S^{-1} of CEO-NE-Based NEG Stored at Refrigeration ($5 \pm 3^\circ\text{C}$) and Ambient Conditions

Storage time	Evaluation Parameters					
	Refrigeration Conditions ($5 \pm 3^\circ\text{C}$)			Ambient Conditions		
	Drug Retention %	pH	η (cP) at γ of 192 s^{-1}	Drug Retention %	pH	η (cP) at γ of 192 s^{-1}
Zero time	100.00 \pm 0.00	4.51 \pm 0.01	6545.31 \pm 156.89	100.00 \pm 0.00	4.51 \pm 0.01	6545.31 \pm 156.89
1 month	100.40 \pm 1.57	4.49 \pm 0.01	6545.31 \pm 156.89	94.88 \pm 0.63	4.46 \pm 0.03	4992.19 \pm 156.89*
2 months	99.99 \pm 2.51	4.49 \pm 0.02	6323.44 \pm 156.89	91.55 \pm 0.95*	4.48 \pm 0.02	4548.44 \pm 156.88*
3 months	98.22 \pm 0.38	4.52 \pm 0.01	6212.50 \pm 0.00	91.11 \pm 3.47*	4.50 \pm 0.03	4326.56 \pm 156.89*
4 months	98.22 \pm 3.14	4.53 \pm 0.02	6101.56 \pm 156.88	89.66 \pm 2.35*	4.85 \pm 0.04*	4104.69 \pm 156.89*
5 months	96.55 \pm 2.98	4.54 \pm 0.01	5990.62 \pm 0.00	75.85 \pm 1.79*	4.75 \pm 0.01*	3882.81 \pm 156.89*
6 months	96.29 \pm 2.48 [#]	4.55 \pm 0.03 [#]	5990.62 \pm 313.78 [#]	65.48 \pm 1.35*	4.77 \pm 0.01*	3328.12 \pm 313.78*

Notes: Each value represents the mean \pm SD (n=3). *Significant at $p < 0.05$ monthly vs initial. [#]Significant at $p < 0.05$ refrigeration vs ambient conditions after 6 months. **Abbreviations:** CEO, clove essential oil; cP, centipoise; NE, nanoemulsion; NEG, nanoemulgel; η , viscosity; γ , shear rate.

could be useful in the treatment of skin inflammatory diseases.^{57–59}

Histopathological Evaluation

Compared with the skin from normal control mice group (Figure 10A), histopathological examination of mice skin tissues exposed to croton oil alone revealed epidermal damage, dermal congestion and edema in addition to marked inflammatory cells infiltration mainly polymorphonuclear (PMN) leukocytes in epidermis and dermis (Figure 10B). Once topical treatment with CEO alone, CEO-NE-based NEG or plain-NE-based NFs did not significantly reduce the harmful effect of croton oil on the skin where the separation of the epidermis from the basement membrane, PMN cells aggregation in epidermis and dermis with dermal congestion and edema were observed (Figure 10C, D and G). Epidermal damage started to disappear in plain-NE-based NEG treated mice with a mild reduction in dermal congestion, edema and PMN cells infiltration (Figure 10E). Interestingly, in case of twice application of CEO-NE-based NEG, much more decreased congestion, edema and PMN cells infiltration in the dermis were noticed (Figure 10F). Meanwhile, once application of CEO-NE-based NFs remarkably inhibited the phlogistic hallmarks of congestion, edema, and PMN cells infiltration induced in the skin by croton oil (Figure 10H).

IHC Evaluation of COX-2 Expression

In the current study, IHC examination was implemented to further clarify the anti-inflammatory activity of the investigated formulae by evaluating the expression level of COX-2 as a key mediator of inflammation pathways.^{60,61}

As shown in Figure 11, COX-2 was positively stained in epidermal cells from all experimental groups (Figure 11A–H). However, positive signal against COX-2 was markedly increased in the skin of mice group treated with croton oil only (Figure 11B). Groups treated with once application of pure CEO, CEO-NE-based NEG or plain-NE-based NFs experienced an increased number of stained PMN cells infiltrating epidermis and dermis (Figure 11C, D and G). Following twice application regimen, the positive signal against COX-2 decreased in skin of plain-NE-based NEG treated group (Figure 11E) and decreased much more in CEO-NE-based NEG treated one (Figure 11F). Since the inflammatory process was prominently suppressed by once treatment with CEO-NE-based NFs formula, the IHC staining of COX-2 appeared as in normal control mice (Figure 11H).

Statistical analysis of the inflammatory and IHC scores of the experimental groups is illustrated in Figure 12. Both groups treated with CEO-NE-based NEG (twice application) and CEO-NE-based NFs (once application) disclosed a significant decrement ($p < 0.05$) in the inflammatory and IHC scores when compared with croton oil or pure CEO treated mice reflecting their superlative anti-inflammatory activity along with relatively higher efficacy of medicated NFs than that of medicated NEG.

In this study, the anti-inflammatory activity of pure CEO and its pharmaceutical delivery systems against croton oil-induced skin inflammation was assessed. Croton oil is a phlogistic agent containing phorbol esters, mainly 12-O-tetradecanoylphorbol-13-acetate (TPA), as irritant agents. Once topical application of croton oil triggers significant inflammatory responses characterized by edema, vascular

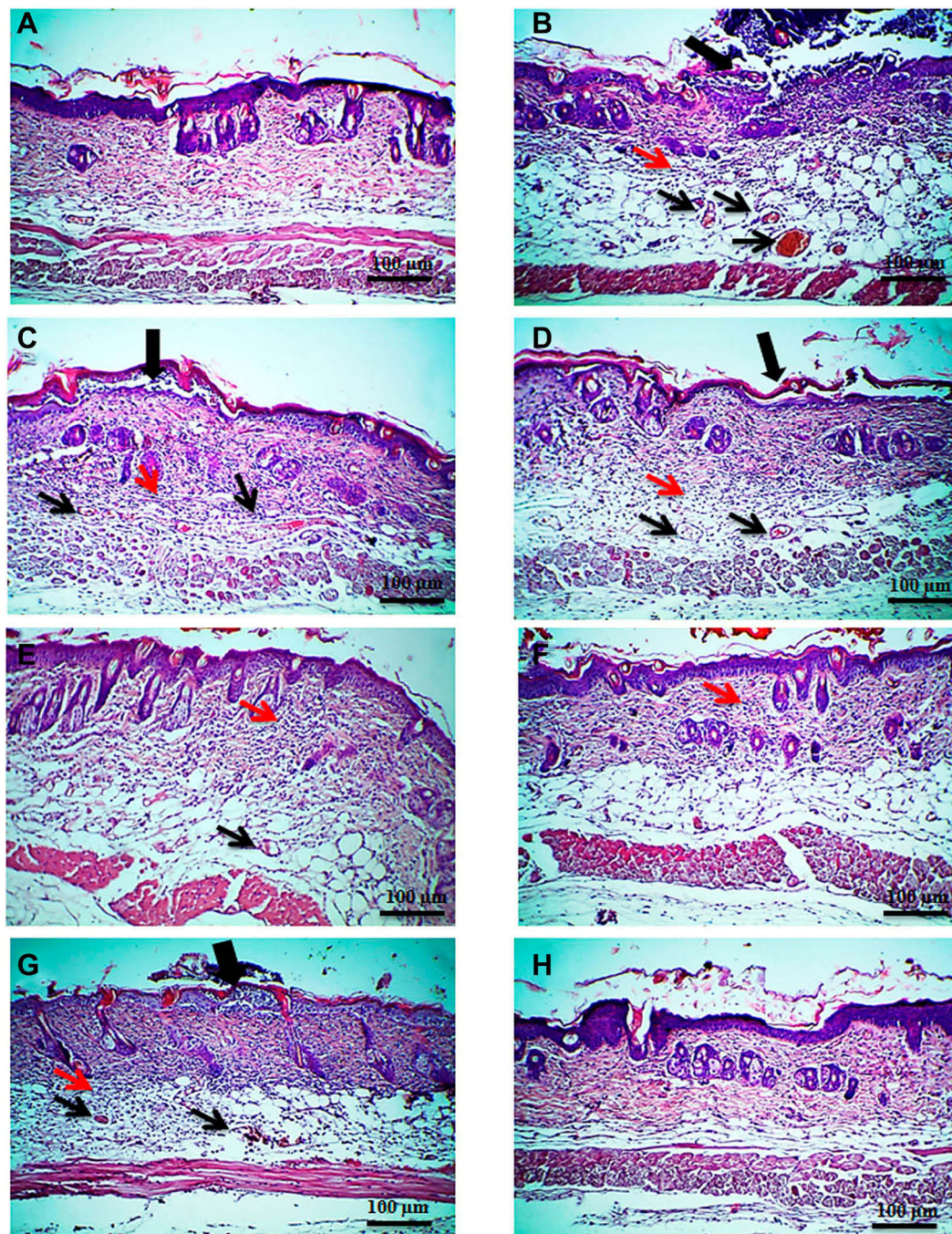


Figure 10 Photomicrographs of histopathological evaluation of the anti-inflammatory activity of the investigated formulae.

Notes: (A) normal control group, (B) croton oil-treated group, (C) pure CEO group (once application), (D) CEO-NE-based NEG (once application), (E) plain-NE-based NEG (twice application), (F) CEO-NE-based NEG (twice application), (G) plain-NE-based NFs (once application), and (H) CEO-NE-based NFs (once application). Thick black arrow points to epidermal damage with marked PMN cells infiltration, thin red arrow points to PMN cells infiltration in dermis, and thin black arrow points to congested blood vessel. H&E, X: 100 bar: 100 µm.

Abbreviations: CEO, clove essential oil; H&E, hematoxylin and eosin; NE, nanoemulsion; NEG, nanoemulgel; NFs, nanofibers; PMN, polymorphonuclear cells.

permeability increment, PMN leukocytes (mainly neutrophils) infiltration, protein kinase C (PKC) activation, prostaglandins (PGs) and leukotrienes production, and several inflammatory mediators induction involving overexpression of COX-2.^{57,58,62}

Although several inflammatory mediators are involved in the inflammation process, several lines of evidence suggested that overexpression of COX-2, a vital key cytokine-inducible enzyme responsible for production of PGs, is robustly implicated in the pathogenesis of inflammatory diseases. Indeed,

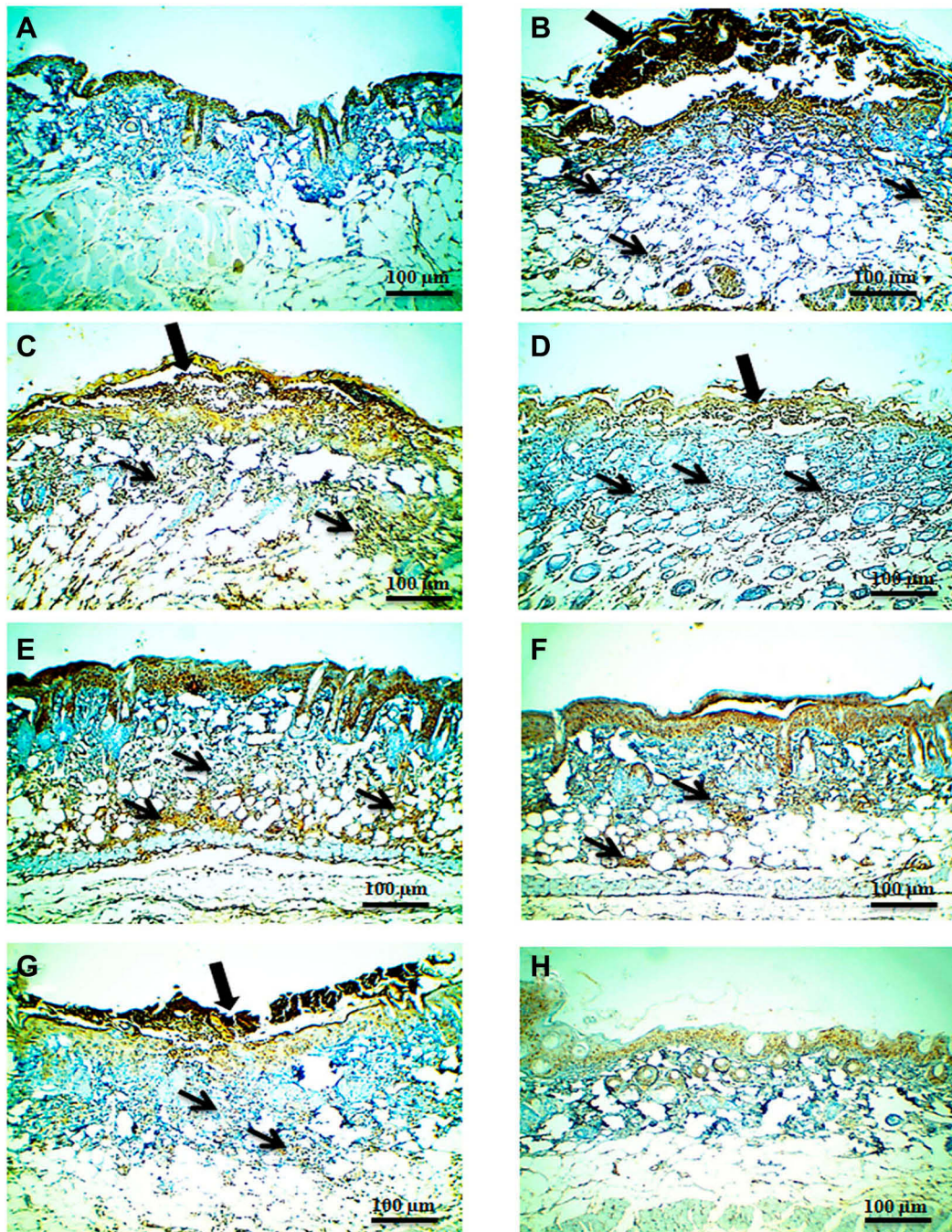


Figure 11 Photomicrographs of IHC evaluation of COX-2 expression level of the investigated formulae.

Notes: (A) normal control group, (B) croton oil-treated group, (C) pure CEO group (once application), (D) CEO-NE-based NEG (once application), (E) plain-NE-based NEG (twice application), (F) CEO-NE-based NEG (twice application), (G) plain-NE-based NFs (once application), and (H) CEO-NE-based NFs (once application). Thick black arrow points to positively stained PMN cells infiltration in epidermis, and thin black arrows point to positively stained PMN cells infiltration in dermis. IHC counterstained with Mayer's hematoxylin, X: 100 bar: 100 µm.

Abbreviations: CEO, clove essential oil; COX-2, cyclooxygenase-2; IHC, immunohistochemical; NE, nanoemulsion; NEG, nanoemulgel; NFs, nanofibers; PMN, polymorphonuclear cells.

nonsteroidal anti-inflammatory drugs (NSAIDs) have been reported to alleviate the inflammation via their effect as COX-2 inhibitors.^{60,61} However, their long-term use either orally or topically is accompanied with serious health

issues.^{63,64} Consequently, many endeavors have been targeted to explore COX-2 inhibitors with minimal adverse effects, particularly from natural origin. Fortunately, among essential oils, CEO containing eugenol as a predominant

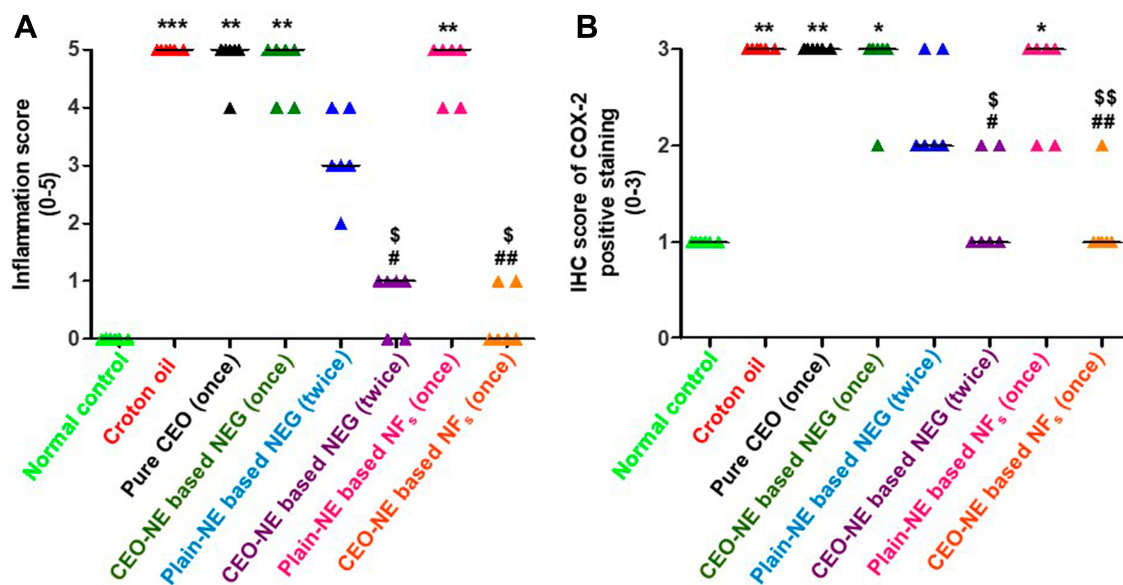


Figure 12 Statistical analysis of inflammation scores (A) and IHC scores (B) in skin from experimental groups (six animals/group).

Notes: Kruskal–Wallis test (nonparametric test) was applied followed by Dunn multiple comparison test. * $p < 0.05$, ** $p < 0.01$ and *** $p < 0.001$ vs normal control group. # $p < 0.05$ and ## $p < 0.01$ vs croton oil group. \$ $p < 0.05$ and \$\$ $p < 0.01$ vs pure CEO group.

Abbreviations: CEO, clove essential oil; IHC, immunohistochemical.

component was very potent in suppressing COX-2 in lipopolysaccharide (LPS)-induced mouse macrophage RAW264.7 cell line as well as in LPS-induced human macrophage U937 cell line.^{65–67} Besides, the previous study demonstrated that the anti-inflammatory activity of CEO was comparable with that of NSAIDs such as etodolac and indomethacin.⁶⁸

From a clinical point of view, the development of topical pharmaceutical delivery systems for CEO to potentiate its anti-inflammatory activity as well as improve patient applicability is a challenge issue. The current study paved the way to achieve such goal by fabricating novel NEG and NFs delivery systems for topical application of CEO. According to the above mentioned *in vivo* data, the potentiated anti-inflammatory activity of such medicated formulae (CEO-NE-based NEG and CEO-NE-based NFs) was clearly established.

Regarding CEO-NE-based NEG, the gel polymeric matrix played an important role due to their proper rheological property, bioadhesive and penetration enhancement characteristics (mainly CS)⁵³ as well as the anti-inflammatory activity (particularly CS and GA), via down-regulation of several inflammatory mediators including COX-2, that may act synergistically with that of CEO.^{69–73} In case of CEO-NE-based NFs, until this moment, no articles were published concerning any anti-inflammatory activity for PVA. Therefore, the low degradation rate property of

polymeric PVA NFs could mainly contribute to CEO retention and accumulation in the skin layers (as a depot) for a prolonged period, and hence sustaining its permeation with reduced systemic effect.⁵⁴ Additionally, there are two common factors in both medicated formulae. The first one is the CEO-NE system with distinctive characteristics such as nanometric size that facilitates its cellular uptake by immune cells, like macrophages, in the inflamed tissues⁷⁴ as well as penetration enhancement ability conferred by the surfactant (tween-80[®]) as one of its components, therefore augmenting the drug cutaneous permeation.^{75–78} The second factor is the permeation pattern of both formulae either controlled (NEG) or sustained (NFs) that has a great influence in decreasing the frequency of dosing at the application site, thence improving the patient compliance for the treatment regimen as well as being cost-effective for prospective commercial production on large scale.

Skin Irritation Test

Skin irritation test was performed as an important requisite to assess the probability of any irritation episodes resulting from topical application of the developed formulae. Histopathological examination of skin from formalin treated mice, as a standard irritant group, revealed an acute inflammation characterized by extensive congestion, edema and PMN cells infiltration in dermis particularly around capillaries (Figure 13B) in comparison with normal skin control

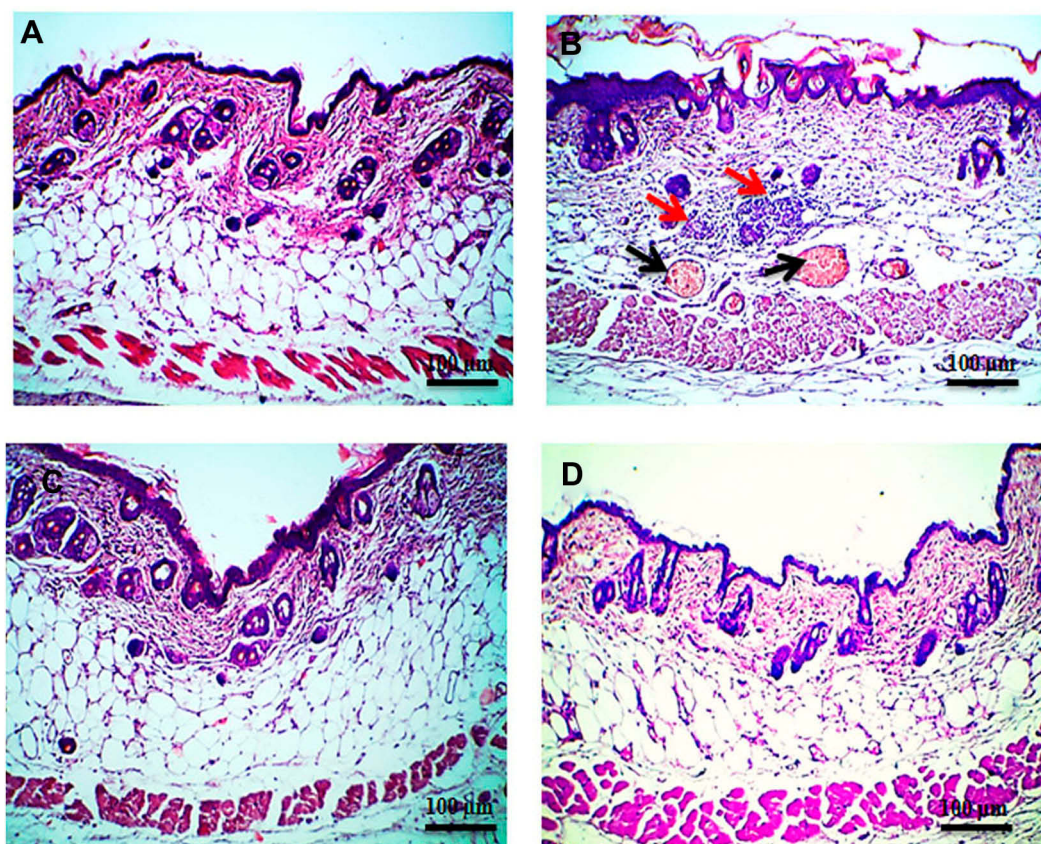


Figure 13 Photomicrographs of histopathological evaluation of skin irritation test.

Notes: (A) normal control mice, (B) formalin treated mice, (C) CEO-NE-based NEG (twice application), and (D) CEO-NE-based NFs (once application). Thin red arrow points to PMN cells infiltration in dermis and thin black arrow points to congested blood vessel. H&E, X: 100 bar: 100 µm.

Abbreviations: CEO, clove essential oil; H&E, hematoxylin and eosin; NE, nanoemulsion; NEG, nanoemulgel; NFs, nanofibers; PMN, polymorphonuclear cells.

group (Figure 13A). Contrary, normal histopathological integrity of mice skin was evident in CEO-NE-based NEG (twice application) and CEO-NE-based NFs (once application) treated groups (Figure 13C and D) indicating their cutaneous safety profile along with foreseeable patient tolerability and compliance for therapeutic use.

Conclusion

The current study confers a bright spark on the establishment of novel controlled release nanoparticulate systems, NEG besides NFs, for CEO topical application with potentiated anti-inflammatory activity. Taguchi's model was employed to optimize the DMPs of the prepared blank hydrogel matrices for further formulation into CEO-NE-based NEG. Moreover, CEO-NE-based NFs was successfully prepared by electrospinning technique using CEO-NE and PVA. Complete dispersion of CEO-NE in the polymeric matrices of the prepared formulae was revealed by FT-IR and DSC results. Both formulae revealed high stability upon storage at $5 \pm 3^\circ\text{C}$ for 6 months. The ex vivo skin permeation data of

CEO from the investigated delivery systems elucidated that CEO-NE-based NFs can sustain the penetration of CEO through the skin when compared with CEO-NE-based NEG. Topical treatment with CEO-NE-based NEG (twice application) and CEO-NE-based NFs (once application) triggered a superlative anti-inflammatory activity against croton oil-induced mouse skin inflammation model comparably with the control pure CEO that was asserted by histopathological and IHC studies. Also, in vivo skin irritation test of the topically applied systems reflected their cutaneous safety profile. These encouraging preclinical data pave the way for prospective clinical investigation of the developed phytopharmaceutical nanoparticulate systems as promising and safe topical treatment regimens for inflammatory disorders instead of the marketed NSAIDs that exhibited drawbacks.

Acknowledgment

The authors would like to express their deepest gratitude and thankfulness to Dr Walaa Awadin, Associate Professor of Pathology, Department of Pathology, Faculty of

Veterinary Medicine, Mansoura University, Egypt for histopathological and immunohistochemical examination.

Disclosure

The authors declare no conflicts of interest in this work.

References

- Caster JM, Patel AN, Zhang T, Wang A. Investigational nanomedicines in 2016: a review of nanotherapeutics currently undergoing clinical trials. *Wiley Interdiscip Rev Nanomed Nanobiotechnol*. 2017;9(1):9e1416. doi:10.1002/wnan.1416
- Sengupta P, Chatterjee B. Potential and future scope of nanoemulgel formulation for topical delivery of lipophilic drugs. *Int J Pharm*. 2017;526(1–2):353–365. doi:10.1016/j.ijpharm.2017.04.068
- Manjanna KM, Pramod Kumar TM, Shivakumar B. Natural polysaccharide hydrogels as novel excipients for modified drug delivery systems: a review. *Int J ChemTech Res*. 2010;2(1):509–525.
- Kriegel C, Kit KM, McClements DJ, Weiss J. Nanofibers as carrier systems for antimicrobial microemulsions. II. Release characteristics and antimicrobial activity. *J Appl Polym Sci*. 2010;118(5):2859–2868. doi:10.1002/app.32563
- Cui Z, Zheng Z, Lin L, et al. Electrospinning and crosslinking of polyvinyl alcohol/chitosan composite nanofiber for transdermal drug delivery. *Adv Polym Technol*. 2018;37(6):1917–1928. doi:10.1002/adv.21850
- Jabeen S, Hanif MA, Khan MM, Qadric RWK. Natural products sources and their active compounds on disease prevention: a review. *IJCBS*. 2014;6:76–83.
- Anwer MK, Jamil S, Ibnouf EO, Shakeel F. Enhanced antibacterial effects of clove essential oil by nanoemulsion. *J Oleo Sci*. 2014;63(4):347–354. doi:10.5650/jos.ess13213
- Shahavi MH, Hosseini M, Jahanshahi M, Meyer RL, Darzi GN. Clove oil nanoemulsion as an effective antibacterial agent: taguchi optimization method. *Desalin Water Treat*. 2016;57(39):18379–18390. doi:10.1080/19443994.2015.1092893
- de Meneses AC, Sayer C, Puton BMS, Cansian RL, Araújo PHH, de Oliveira D. Production of clove oil nanoemulsion with rapid and enhanced antimicrobial activity against gram-positive and gram-negative bacteria. *J Food Process Eng*. 2019;42(6):e13209. doi:10.1111/jfpe.13209
- Nirmala MJ, Durai L, Gopakumar V, Nagarajan R. Anticancer and antibacterial effects of a clove bud essential-oil based nanoscale emulsion system. *Int J Nanomedicine*. 2019;14:6439–6450. doi:10.2147/IJN.S211047
- Tonglairoum P, Ngawhirunpat T, Rojanarata T, Kaomongkolgit R, Opanasopit P. Fabrication and evaluation of nanostructured herbal oil/hydroxypropyl- β -cyclodextrin/polyvinylpyrrolidone mats for denture stomatitis prevention and treatment. *AAPS PharmSciTech*. 2016;17(6):1441–1449. doi:10.1208/s12249-016-0478-2
- Rafiq M, Hussain T, Abid S, Nazir A, Masood R. Development of sodium alginate/PVA antibacterial nanofibers by the incorporation of essential oils. *Mater Res Express*. 2018;5(3):035007. doi:10.1088/2053-1591/aab0b4
- Madan SS, Wasewar KL. Optimization for benzenoacetic acid removal from aqueous solution using CaO₂ nanoparticles based on Taguchi method. *J Appl Res Technol*. 2017;15(4):332–339. doi:10.1016/j.jart.2017.02.007
- Zakaria AS, Afifi SA, Elkhodairy KA. Newly developed topical cefotaxime sodium hydrogels: antibacterial activity and *in vivo* evaluation. *Biomed Res Int*. 2016;2016:ID 6525163. doi:10.1155/2016/6525163
- Lei L, He Z, Chen H, McClements DJ, Li B, Li Y. Microstructural, rheological, and antibacterial properties of cross-linked chitosan emulgels. *RSC Adv*. 2015;5(121):100114–100122. doi:10.1039/C5RA19757K
- Celebioglu A, Yildiz ZI, Uyar T. Fabrication of electrospun eugenol/cyclodextrin inclusion complex nanofibrous webs for enhanced antioxidant property, water solubility, and high temperature stability. *J Agric Food Chem*. 2018;66(2):457–466. doi:10.1021/acs.jafc.7b04312
- Ahmed OAA, Rizq WY. Finasteride nano-transferosomal gel formula for management of androgenetic alopecia: ex vivo investigational approach. *Drug Des Devel Ther*. 2018;12:2259–2265. doi:10.2147/DDDT.S171888
- Elmataeeshy ME, Sokar MS, Bahey-El-Din M, Shaker DS. Enhanced transdermal permeability of Terbinafine through novel nanoemulgel formulation; development, *in vitro* and *in vivo* characterization. *Future J Pharm Sci*. 2018;4(1):18–28. doi:10.1016/j.fjps.2017.07.003
- Higuchi T. Mechanism of sustained action medication: theoretical analysis of rate of release of solid drugs dispersed in solid matrix. *J Pharm Sci*. 1963;52:1145–1149. doi:10.1002/jps.2600521210
- Korsmeyer RW, Gurny R, Doelker E, Buri P, Peppas NA. Mechanism of solute release from porous hydrophilic polymers. *Int J Pharm*. 1983;15(1):25–35. doi:10.1016/0378-5173(83)90064-9
- Aithal GC, Nayak UY, Mehta C, et al. Localized *in situ* nanoemulgel drug delivery system of quercetin for periodontitis: development and computational simulations. *Molecules*. 2018;23(6):E1363. doi:10.3390/molecules23061363
- Shwaireb MH. Inflammatory effects of the tumor promoter croton oil in BALB/c mice skin. *Oncol Rep*. 1995;2(1):133–135. doi:10.3892/or.2.1.133
- Anter HM, Abu Hashim II, Awadin W, Meshali MM. Novel anti-inflammatory film as a delivery system for the external medication with bioactive phytochemical “Apocynin”. *Drug Des Devel Ther*. 2018;12:2981–3001. doi:10.2147/DDDT.S176850
- Ramadan E, Borg T, Abdelghani GM, Saleh NM. Design and *in vivo* pharmacokinetic study of a newly developed lamivudine transdermal patch. *Future J Pharm Sci*. 2018;4(2):166–174. doi:10.1016/j.fjps.2018.03.002
- Esmaili F, Rajabnejhad S, Partoazar AR, et al. Antiinflammatory effects of eugenol nanoemulsion as a topical delivery system. *Pharm Dev Technol*. 2016;21(7):887–893. doi:10.3109/10837450.2015.1078353
- Bancroft JD, Gamble M. *Theory and Practice of Histological Techniques*. 5th ed. London, UK: Churchill Livingstone; 2007:125–138.
- Bang JS, Choi HM, Sur BJ, et al. Anti-inflammatory and antiarthritic effects of piperine in human interleukin 1 β -stimulated fibroblast-like synoviocytes and in rat arthritis models. *Arthritis Res Ther*. 2009;11(2):R49. doi:10.1186/ar2662
- Hussein SZ, Yusoff KM, Makpol S, Yusof YAM. Gelam honey attenuates carrageenan-induced rat paw inflammation via NF- κ B pathway. *PLoS One*. 2013;8(8):e72365. doi:10.1371/journal.pone.0072365
- Fisher ER, Anderson S, Dean S, et al. Solving the dilemma of the immunohistochemical and other methods used for scoring estrogen receptor and progesterone receptor in patients with invasive breast carcinoma. *Cancer*. 2005;103(1):164–173. doi:10.1002/cncr.20761
- Anbar HS, Shehatou GSG, Suddek GM, Gameil NM. Comparison of the effects of levocetirizine and losartan on diabetic nephropathy and vascular dysfunction in streptozotocin-induced diabetic rats. *Eur J Pharmacol*. 2016;780:82–92. doi:10.1016/j.ejphar.2016.03.035
- Shende PK, Gaud RS, Bakal R, Yeole Y. Clove oil emulsified buccal patch of serratiopeptidase for controlled release in toothache. *J Bioequiv Availab*. 2016;8(3):134–139. doi:10.4172/jbb.1000283
- Lacerda CV, Carvalho MJS, Rattton AR, Soares IP, Borges LEP. Synthesis of triacetin and evaluation on motor. *J Braz Chem Soc*. 2015;26(8):1625–1631. doi:10.5935/0103-5053.20150133
- Arun P, Pudi SM, Biswas P. Acetylation of glycerol over sulfated alumina: reaction parameter study and optimization using response surface methodology. *Energy Fuels*. 2016;30(1):584–593. doi:10.1021/acs.energyfuels.5b01901

34. Karataş A, Bekmezci S. Evaluation and enhancement of physical stability of semi-solid dispersions containing piroxicam into hard gelatin capsules. *Acta Pol Pharm.* 2013;70(5):883–897.
35. Kura AU, Hussein-Al-Ali SH, Hussein MZ, Fakurazi S. Preparation of tween 80-Zn/Al-levodopa-layered double hydroxides nanocomposite for drug delivery system. *Sci World J.* 2014;2014:ID 104246. doi:10.1155/2014/104246
36. Rachmawati H, Budiputra DK, Mauludin R. Curcumin nanoemulsion for transdermal application: formulation and evaluation. *Drug Dev Ind Pharm.* 2015;41(4):560–566. doi:10.3109/03639045.2014.884127
37. Izadiyan Z, Basri M, Masoumi HRF, Karjiban RA, Salim N, Shameli K. Modeling and optimization of nanoemulsion containing sorafenib for cancer treatment by response surface methodology. *Chem Cent J.* 2017;11:21. doi:10.1186/s13065-017-0248-6.
38. Celep GK, Dincer K. Application of taguchi method for the synthesis of nano-sized TiO₂ powders by acid-used sol-gel method. *Anadolu Univ J of Sci Technol Appl Sci Eng.* 2017;18(3):705–712.
39. Hadgraft J. Skin, the final frontier. *Int J Pharm.* 2001;224(1–2):1–18. doi:10.1016/s0378-5173(01)00731-1
40. Abdul Rasool BK, Abu-Gharbich EF, Fahmy SA, Saad HS, Khan SA. Development and evaluation of ibuprofen transdermal gel formulations. *Trop J Pharm Res.* 2010;9(4):355–363.
41. El-Hefian EA, Elgannoudi ES, Mainal A, Yahaya AH. Characterization of chitosan in acetic acid: rheological and thermal studies. *Turk J Chem.* 2010;34:47–56. doi:10.3906/kim-0901-38
42. Mudgil D, Barak S, Khatkar BS. Guar gum: processing, properties and food applications – A review. *J Food Sci Technol.* 2014;51(3):409–418. doi:10.1007/s13197-011-0522-x
43. Modrzejewska Z, Nawrotek K, Zarzycki R, Douglas T. Structural characteristics of thermosensitive chitosan glutamate hydrogels. *PCACD.* 2013;17:93–106.
44. Bianchera A, Salomi E, Pezzanera M, Ruwet E, Bettini R, Elviri L. Chitosan hydrogels for chondroitin sulphate controlled release: an analytical characterization. *J Anal Methods Chem.* 2014;2014:ID 808703. doi:10.1155/2014/808703
45. Mudgil D, Barak S, Khatkar BS. X-ray diffraction, IR spectroscopy and thermal characterization of partially hydrolyzed guar gum. *Int J Biol Macromolec.* 2012;50(4):1035–1039. doi:10.1016/j.ijbiomac.2012.02.031
46. Sharma R, Kaith BS, Kalia S, et al. Biodegradable and conducting hydrogels based on guar gum polysaccharide for antibacterial and dye removal applications. *J Environ Manage.* 2015;162:37–45. doi:10.1016/j.jenvman.2015.07.044
47. Borodina T, Grigoriev D, Markvicheva E, Möhwald H, Shchukin D. Vitamin E microspheres embedded within a biocompatible film for planar delivery. *Adv Eng Mater.* 2011;13(3):B123–B130. doi:10.1002/adem.201080047
48. Cekić ND, Đorđević SM, Savić SR, Savić SD. A full factorial design in the formulation of diazepam parenteral nanoemulsions: physico-chemical characterization and stability evaluation. *Adv Technol.* 2015;4(1):69–77. doi:10.5937/savteh1501069C
49. Dhibar M, Chakraborty S, Khandai M. Curcumin loaded in-situ nanoemulgel: a unique dosage form for ophthalmic drug delivery. *Int J Pharm Sci Rev Res.* 2018;48(1):141–147.
50. Han X, Chen S, Hu X. Controlled-release fertilizer encapsulated by starch/polyvinyl alcohol coating. *Desalination.* 2009;240(1–3):21–26. doi:10.1016/j.desal.2008.01.047
51. Alhosseini SN, Moztarzadeh F, Mozafari M, et al. Synthesis and characterization of electrospun polyvinyl alcohol nanofibrous scaffolds modified by blending with chitosan for neural tissue engineering. *Int J Nanomedicine.* 2012;7:25–34. doi:10.2147/IJN.S25376
52. Gökmeşe F, Uslu I, Aytimur A. Preparation and characterization of PVA/PVP nanofibers as promising materials for wound dressing. *Polym Plast Technol Eng.* 2013;52(12):1259–1265. doi:10.1080/03602559.2013.814144
53. Bussio JI, Molina-Perea C, González-Aramundiz JV. Lower-sized chitosan nanocapsules for transcutaneous antigen delivery. *Nanomaterials.* 2018;8:E659. doi:10.3390/nano8090659
54. Azarbayjani AF, Venugopal JR, Ramakrishna S, Lim PFC, Chan YW, Chan SY. Smart polymeric nanofibers for topical delivery of levothyroxine. *J Pharm Pharmaceut Sci.* 2010;13(3):400–410. doi:10.18433/j3ts3g
55. Arora R, Aggarwal G, Harikumar SL, Kaur K. Nanoemulsion based hydrogel for enhanced transdermal delivery of ketoprofen. *Adv Pharm.* 2014;2014:ID 468456. doi:10.1155/2014/468456
56. Ghitman J, Stan R, Ghebaur A, Cecoltan S, Vasile E, Iovu H. Novel PEG-modified hybrid PLGA-vegetable oils nanostructured carriers for improving performances of indomethacin delivery. *Polymers.* 2018;10(6):579. doi:10.3390/polym10060579
57. Shin S, Joo SS, Park D, et al. Ethanol extract of *Angelica gigas* inhibits croton oil-induced inflammation by suppressing the cyclooxygenase - prostaglandin pathway. *J Vet Sci.* 2010;11(1):43–50. doi:10.4142/jvs.2010.11.1.43
58. Luo H, Lv XD, Wang GE, Li YF, Kurihara H, He RR. Anti-inflammatory effects of anthocyanins-rich extract from bilberry (*Vaccinium myrtillus* L.) on croton oil-induced ear edema and Propionibacterium acnes plus LPS-induced liver damage in mice. *Int J Food Sci Nutr.* 2014;65(5):594–601. doi:10.3109/09637486.2014
59. Raposo S, Tavares R, Gonçalves L, Simões S, Urbano M, Ribeiro HM. Mometasone furoate-loaded cold processed oil-in-water emulsions: in vitro and in vivo studies. *Drug Deliv.* 2015;22(4):562–572. doi:10.3109/10717544.2013.871086
60. Ricciotti E, FitzGerald GA. Prostaglandins and inflammation. *Arterioscler Thromb Vasc Biol.* 2011;31(5):986–1000. doi:10.1161/ATVBAHA.110.207449
61. Gandhi J, Khera L, Gaur N, Paul C, Kaul R. Role of modulator of inflammation cyclooxygenase-2 in gammaherpesvirus mediated tumorigenesis. *Front Microbiol.* 2017;8:538. doi:10.3389/fmicb.2017.00538
62. Rahman S, Ansari RA, Rehman H, Parvez S, Raisuddin S. Nordihydroguaiaretic acid from creosote bush (*Larrea tridentata*) mitigates 12-O-tetradecanoylphorbol-13-acetate-induced inflammatory and oxidative stress responses of tumor promotion cascade in mouse skin. *Evid Based Complement Alternat Med.* 2011;2011:ID 734785. doi:10.1093/ecam/nep076
63. Haroutiunian S, Drennan DA, Lipman AG. Topical NSAID therapy for musculoskeletal pain. *Pain Med.* 2010;11(4):535–549. doi:10.1111/j.1526-4637.2010.00809.x
64. Sinha M, Gautam L, Shukla PK, Kaur P, Sharma S, Singh TP. Current perspectives in NSAID-induced gastropathy. *Mediators Inflamm.* 2013;2013(ID):258209. doi:10.1155/2013/258209
65. Hong CH, Hur SK, Oh OJ, Kim SS, Nam KA, Lee SK. Evaluation of natural products on inhibition of inducible cyclooxygenase (COX-2) and nitric oxide synthase (iNOS) in cultured mouse macrophage cells. *J Ethnopharmacol.* 2002;83(1–2):153–159. doi:10.1016/s0378-8741(02)00205-2
66. Kim SS, Oh OJ, Min HY, et al. Eugenol suppresses cyclooxygenase-2 expression in lipopolysaccharide-stimulated mouse macrophage RAW264.7 cells. *Life Sci.* 2003;73(3):337–348. doi:10.1016/s0024-3205(03)00288-1
67. Lee YY, Hung SL, Pai SF, Lee YH, Yang SF. Eugenol suppressed the expression of lipopolysaccharide-induced proinflammatory mediators in human macrophages. *J Endod.* 2007;33(6):698–702. doi:10.1016/j.joen.2007.02.010
68. Öztürk A, Özbek H. The anti-inflammatory activity of eugenia caryophyllata essential oil: an animal model of anti-inflammatory activity. *Eur J Gen Med.* 2005;2(4):159–163. doi:10.29333/ejgm/82334
69. Chou TC, Fu E, Shen EC. Chitosan inhibits prostaglandin E2 formation and cyclooxygenase-2 induction in lipopolysaccharide-treated RAW 264.7 macrophages. *Biochem Biophys Res Commun.* 2003;308(2):403–407. doi:10.1016/s0006-291x(03)01407-4

70. Ali BH, Al-Husseni I, Beegam S, et al. Effect of gum arabic on oxidative stress and inflammation in adenine-induced chronic renal failure in rats. *PLoS One*. 2013;8(2):e55242. doi:10.1371/journal.pone.0055242
71. Kim S. Competitive biological activities of chitosan and its derivatives: antimicrobial, antioxidant, anticancer, and anti-inflammatory activities. *Int J Polym Sci*. 2018;2018(ID):1708172. doi:10.1155/2018/1708172
72. Xiong H, Wu M, Zou H, et al. Chitosan inhibits inflammation and adipogenesis of orbital fibroblasts in Graves ophthalmopathy. *Mol Vis*. 2018;24:509–517.
73. Hamid M, Abdulrahim Y, Liu D, Qian G, Khan A, Huang K. The hepatoprotective effect of selenium-enriched yeast and gum arabic combination on carbon tetrachloride-induced chronic liver injury in rats. *J Food Sci*. 2018;83(2):525–534. doi:10.1111/1750-3841.14030
74. Cortivo R, Vindigni V, Iacobellis L, Abatangelo G, Pinton P, Zavan B. Nanoscale particle therapies for wounds and ulcers. *Nanomedicine*. 2010;5(4):641–656. doi:10.2217/nmm.10.32
75. Akhtar N, Rehman MU, Khan HMS, Rasool F, Saeed T, Murtaza G. Penetration enhancing effect of polysorbate 20 and 80 on the *in vitro* percutaneous absorption of L-ascorbic acid. *Trop J Pharm Res*. 2011;10(3):281–288. doi:10.4314/tjpr.v10i3.1
76. Ahmad N, Ahmad FJ, Bedi S, Sharma S, Umar S, Ansari MA. A novel nanoformulation development of eugenol and their treatment in inflammation and periodontitis. *Saudi Pharm J*. 2019;27(6):778–790. doi:10.1016/j.jsps.2019.04.014
77. Ahmad N, Alam MA, Ahmad FJ, et al. Ultrasonication techniques used for the preparation of novel eugenol-nanoemulsion in the treatment of wounds healings and anti-inflammatory. *J Drug Deliv Sci Technol*. 2018;46:461–473. doi:10.1016/j.jddst.2018.06.003
78. Ahmad N, Ahmad R, Al-Qudaihi A, et al. Preparation of a novel curcumin nanoemulsion by ultrasonication and its comparative effects in wound healing and the treatment of inflammation. *RSC Adv*. 2019;9:20192–20206. doi:10.1039/c9ra03102b

International Journal of Nanomedicine

Dovepress

Publish your work in this journal

The International Journal of Nanomedicine is an international, peer-reviewed journal focusing on the application of nanotechnology in diagnostics, therapeutics, and drug delivery systems throughout the biomedical field. This journal is indexed on PubMed Central, MedLine, CAS, SciSearch®, Current Contents®/Clinical Medicine,

Journal Citation Reports/Science Edition, EMBase, Scopus and the Elsevier Bibliographic databases. The manuscript management system is completely online and includes a very quick and fair peer-review system, which is all easy to use. Visit <http://www.dovepress.com/testimonials.php> to read real quotes from published authors.

Submit your manuscript here: <https://www.dovepress.com/international-journal-of-nanomedicine-journal>